12

FINAL TECHNICAL REPORT
SPONSORED BY
ADVANCED RESEARCH PROJECTS AGENCY
CONTRACT NO. DAHC04-~~71 C 0046~~
74-G-0236

(12)

~~REPORT SUMMARY~~

(9) FINAL TECHNICAL REPORT,

SPONSORED BY

ADVANCED RESEARCH PROJECTS AGENCY

ARPA ORDER NO. 675AM.20

PROGRAM CODE NO. 62301 E

CONTRACT NO. DAHC04-~~71 C 0046~~ 74-G-0236

NAME OF CONTRACTOR: The University of Rochester
College of Engineering & Applied Science
Rochester, New York

TITLE OF PROJECT: (6) New Laser Concepts in the Visible, UV, and Soft X-Ray Region.

PRINCIPAL INVESTIGATOR: (10) Moshe J. Lubin
Professor, Department of Mechanical & Aerospace Sciences and the Institute of Optics
Director, Laboratory for Laser Energetics
Phone (716) 275-5101

(11) 1974

(12) 125p.

(15) DAHC04-74-G-0236

Under ARPA Contract DAHC04-~~71-C-0046~~ 74-G-0236, titled "New Laser Concepts in the Visible, UV, and Soft X-Ray Region", the work described in the following publications was carried out. This summary constitutes the final report under the contract.

(15) DAHC04-74-G-0236, ARPA Order-675

307250

FINAL TECHNICAL REPORT

SPONSORED BY

ADVANCED RESEARCH PROJECTS AGENCY

ARPA ORDER NO. 675AM.20

PROGRAM CODE NO. 62301 E

CONTRACT NO. DAHC04-~~71-C-0046~~ 74-G-0236

NAME OF CONTRACTOR:	The University of Rochester College of Engineering & Applied Science Rochester, New York
TITLE OF PROJECT:	New Laser Concepts in the Visible, UV, and Soft X-Ray Region
PRINCIPAL INVESTIGATOR:	Moshe J. Lubin Professor, Department of Mechanical & Aerospace Sciences and the Institute of Optics Director, Laboratory for Laser Energetics Phone (716) 275-5101
SCIENTIFIC OFFICE:	Physics Division; Army Research Office P.O. Box 12211 Research Triangle Park, North Carolina 2770[illegible]
EFFECTIVE DATE:	July 1, 1974
CONTRACT EXPIRATION DATE:	June 30, 1975
AMOUNT OF CONTRACT:	$60,000

This research was supported by the Advance Research Projects Agency of the Department of Defense and was monitored by the U.S. Army Research Office-Durham under Grant/Contract No. DAHC04-~~71-C-0046.~~ 74-G-0236

The views and conclusions contained in this document are those of the authors and should not be interpreted as necessarily representing the official policies, either expressed or implied, of the Advanced Research Projects Agency or the U.S. Government.

Approved for public release, distribution unlimited.

HIGH INTENSITY X-RAY SPECTRA AND STIMULATED EMISSION FROM LASER PLASMAS †

Report No. 10

by

T. C. Bristow, M. J. Lubin, J. M. Forsyth,
E. B. Goldman, and J. M. Soures

†This work was supported by ARPA under contract DAHC04-~~71-C-0046~~. 74-G-0236
The work was approved for public release and the distribution unlimited.

ABSTRACT

The conversion efficiency of input laser radiation to output soft x-rays from an oxygen doped spherical laser plasma is calculated. Experimental verification has been obtained for one doping concentration. The fast risetime ($<10^{-11}$ sec) of the calculated oxygen line spectra suggests a method of producing a population inversion. A gain of 10^{0}-10^{4}db/cm is shown for the 2s-3p (128Å) transition of OVII.

I. INTRODUCTION

Conversion efficiency of visible radiation from a focused laser beam to high-intensity soft x-ray radiation via laser-produced plasmas has been suggested as an efficient means of generating a desired soft x-ray spectra.[1] A knowledge of the time history of continuum and line components of the x-ray spectra facilitates a determination of electron and ion temperature in the laser plasma. In this letter we report initial theoretical and experimental results of the time history of oxygen x-ray spectra for a small percentage of oxygen impurity in a spherically symmetric plasma. The plasma is produced by focused irradiation of an oxygen-doped deuterium pellet. The calculation of a high conversion efficiency of input laser energy to output energy in soft x-rays, coupled with extremely fast calculated risetimes of the line emission ($<10^{-11}$ sec) immediately suggests that the x-ray line spectra could be used as a pumping source for an x-ray laser. Moreover, efficient electron impact excitation at work in these dense plasmas could be responsible for direct population inversion and subsequent lasing. A calculation demonstrating the possibility of achieving a population inversion at 128Å is presented as an example of this process.

Oxygen was chosen for these studies because the cross-section data is well-known and it goes into solution with deuterium in closely controlled percentages.

Numerical studies of low Z spherical targets lightly doped with heavy elements are readily performed using a one-dimensional Lagrangian computer code.[2] This code was used to study the emission from the

OVI $2s^2S$ - $3p^2p^o$ transition (λ = 150.12Å); the OVII $1s^2\ ^1S$ - $1s2p^1p^o$ (λ = 21.6Å); $1s^2\ ^1S$ - $1s3p^1p^o$ (λ = 18.63Å); $1s2s^1S$ - $1s3p^1p^o$ (λ = 128.25Å) transitions and the OVIII $1s^1S$ - $2p^2p^o$ (λ = 18.97Å) transition.[3] The study was restricted to these configurations because the excitation cross sections and oscillator strengths for these lines are considerably larger than other cross-sections at temperatures characteristic of laser produced plasmas.

Absorption of the incident focused radiation by the spherical plasma is predominantly an inverse bremsstrahlung process, i.e., the absorption exhibits a Z^2 dependence.[4] Hence, the addition of high Z impurities to the plasma leads to a greater overall absorption with elevated electron temperatures. The radiation power density from the plasma consisting of both continuum (free-free, P_{ff}, and bound-free, P_{bf}) and line components, is strongly Z dependent;

$$P_{ff} = 1.5 \times 10^{-32} n_e n_i (kT_e)^{1/2} Z^2 \quad \text{watts/cm}^3 \tag{1}$$

$$P_{bf} = \frac{2Z^2 E_h}{kT_e} \quad P_{ff} \quad \text{watts/cm}^3 \tag{2}$$

where n_e and n_i are the electron and ion number density in cm^{-3}, respectively, kT_e the electron temperature in eV, and E_h the ionization potential of hydrogen. The line radiation from impurity atoms has a Z dependence which is a function of the excitation potential.

We describe the radiation dynamics of the impurity ions by a rate equation for the degree of ionization of a particular state given in terms of ionization and recombination coefficients. Reabsorption of

the emitted radiation is not important in lightly doped laser plasmas because they are optically thin to this calculated soft x-ray spectra. The rate equations are of the form:

$$\frac{dq_j}{dt} = n_e q_{j-1} \langle \sigma v \rangle^i_{j-1} - n_e q_j \left(\langle \sigma v \rangle^i_j + \langle \sigma v \rangle^r_j \right) + n_e q_{j+1} \langle \sigma v \rangle^r_{j+1} , \quad j = 1, 9, \tag{3}$$

where q_j is the fractional ionization of the jth species (q_8 is the hydrogenic ion), and $\langle \sigma v \rangle^i_j$ and $\langle \sigma v \rangle^r_j$ are ionization and recombination cross-sections respectively, averaged over a Maxwellian distribution.[5] The coefficients are

$$\langle \sigma v \rangle^i_j = \frac{2.5 \times 10^{-6} \, \eta (kT_e/x_j)^{1/2}}{x_j^{3/2} \, (1 + kT_e/x_j)} \exp(-x_j/kT_e) \ \text{cm}^3 \ \text{sec}^{-1} \tag{4}$$

$$\langle \sigma v \rangle^r_{j+1} = 5.2 \times 10^{-14} \, z (x_j/kT_e)^{1/2} \left[0.429 + 1/2 \ln (x_j/kT_e) + 0.469 (x_j/kT_e)^{-1/3} \right] + 1.4 \times 10^{-31} z^{-6} n_e (n')^6 \left(\frac{x_j}{kT_e} \right)^2 \times \exp \left[x_j/(n' + 1)^2 kT_e \right] \ \text{cm}^3 \ \text{sec}^{-1} \tag{5}$$

where x_j is the ionization potential, η is the number of equivalent electrons (η=1 for hydrogen, η=2 for helium), z is the effective charge, and n' is the collision limit (n'≃2 for oxygen doped dense plasmas).[6,7] The recombination cross-secion, equation (5), consists of two parts;

the first term is radiation recombination and the second term a three-body recombination cross-section.

The power density from an excited state in the jth species is:

$$P_{Lj}^{ku} = n_e^{\,2} q_j q_o \langle \sigma v \rangle_{ex}^{ku} h\nu \qquad \text{watts/cm}^3 \,, \tag{6}$$

where q_o is the fraction of impurity atoms (with respect to n_e); and

$$\langle \sigma v \rangle_{ex}^{ku} = \frac{6 \times 10^{-6}}{X_u (kT_e)^{1/2}} \, f_{ku} \, \exp(-X_u/kT_e) \ \text{cm}^3/\text{sec}^{-1} \,, \tag{7}$$

where f_{ku} is the absorption oscillator strength for a u to k line transition, and X_u is the excitation potential of the uth state. Implicit in eq. (6) is the assumption that every collisional excitation results in the instantaneous emission of a photon.

A typical calculated time history of an impurity doped spherical pellet heated by an incident 1.06 μm 265 joule laser pulse of 10^{-10} seconds duration is shown in Figures 1 and 2. These calculations were carried out using a two-temperature hydrodynamic, spherically symmetric Lagrangian code which allows for complete energy transfer between species. Figs. 1a and 1b show the density profile and electron temperature vs. the radius of the plasma for various times of interest. In addition to the 100 micron core, initially at solid density, a low density tail is present which has been formed by a prepulse applied to enhance the absorption process.[8]

In Fig. 2a the time history of the various lines is shown. Lines from the OVII and OVIII states exhibit a fast rise ($<10^{-11}$ sec) during the laser heating of the plasma followed by slower decay with the

electron temperature. During the early heating of the plasma, the electron temperature is 10^7 ^oK leading to the emission of the OVII and OVIII lines. As the electron temperature drops to 10^6 ^oK the line emission decreases, because the excitation cross section is proportional to $\exp(-X_u/kT_e)$. The line radiation originates in the outer high-temperature low-density region of the plasma; the cold center core does not contribute to the radiation dynamics at these short times. Fig. 2b gives the energy in each line vs. time. In this calculation the total energy absorbed by the plasma from the incident laser beam is 19.3 joules. The continuum radiation emitted from the deuterium plasma is 1.1 joules whereas the contribution from the impurity species to the continuum for 1% oxygen doping is 0.3 joules.

Experimental confirmation of the high conversion efficiencies to soft x-rays has been made in the case of a 6% oxygen-doped LiD spherical target subjected to a 2 joule 10^{-10} second laser pulse with a prepulse. In the experiment an incident laser pulse was focused on a LiD spherical target by an f/1 aspheric lens. The focal spot size was measured to be less than 50 μm. The x-rays were measured by solid state (PIN-SILICON) and PM-Scintillator detectors. Partially absorbing nickel or aluminum foils were placed in front of the detectors to measure the electron temperature. Charged particle detectors were included to measure the energy absorbed by the plasma, and detectors are included to measure the flux of neutrons from the plasma.

Using the absolute sensitivity of the solid state detector, and the x-ray foil transmission coefficients[9], the conversion efficiency of laser energy to soft x-rays is found to be 0.44%. The numerical code

was used for the experimental case corresponding to 0.3 joules absorbed and the conversion efficiency was calculated to be 0.52% in good agreement with the experimental results.

The following observations can be made from the numerical calculation. First, the risetime of the line emission is very fast ($<10^{-11}$sec). Second, the intensity of the lines depends very strongly on the electron temperature so that in the early phase of plasma heating (where $T_e > T_i$) line radiation is emitted.

Finally, the very rapid non-equilibrium electron impact excitation in oxygen-doped laser plasmas suggests a possible mechanism for population inversion. Referring to the energy level diagram of oxygen, Fig. 3 it is seen that the 2s states in OVII will have negligible cross-section for direct excitation compared to the cross-section for direct excitation of the 2p and 3p states. Therefore, during early times it should be possible to produce an inverted population on the 2s-3p and the 2s-2p transitions. The decay from the 2s-3p transition, characterized by $A \simeq 5.04 \times 10^{10}$ sec^{-1}, is very rapid compared to the rate of spontaneous decay ($A \simeq 2.46 \times 10^{7}$ sec^{-1}) for the 2s-2p transition. The radiation from the shorter wavelength transition should, therefore, inhibit the maintenance of a population inversion at the longer wavelength over a timespan sufficient to permit significant buildup of stimulated emission. We have, therefore, restricted our interest to the 2s-3p transition ($\lambda = 128.25\mathring{A}$).

An estimate of the gain can be made from a calculation of the excitation rate of the 3p level ($X_{3p} = 665$ eV) and an approximation to the stark broadened line profile. For example, the equilibrium electron

impact excitation rate obtained from eq. (7), valid for times longer than 10^{-11} seconds (electron-electron thermalization time at 1.2 KeV), is $C_{eq} = n_e\langle\sigma v\rangle_{ex}$. With the parameters, $n_e \simeq 10^{20} cm^{-3}$, kT_e = 1.2 KeV, we obtain $G_{pq} \simeq 2.4 \times 10^{9} sec^{-1}$. For times shorter than 10^{-11} seconds, the electron impact excitation process must be based on a non-equilibrium cross-section. An extimate of this cross-section may be using a modified Coulomb-Born approximation,

$$\sigma_{ku} = 2.3 \times 10^{-13} f_{ku} \bar{g}/\varepsilon X_u \quad cm^2 \tag{8}$$

giving

$$\langle\sigma v\rangle ne = \frac{4.31 f_{ku}}{X_u \varepsilon_o^{1/2}} \quad cm^3 sec^{-1} \tag{9}$$

where $\bar{g}$ is the effective Gaunt factor ($\bar{g} \simeq .2$), ε is the kinetic energy of the electrons in eV, and ε_o is the peaked energy of the electron in eV.[7,10] Implicit in this expression is the assumption that the electron velocity ditribution is strongly peaked around the value $(2\varepsilon_o/m)^{1/2}$. Using the same parameters, we obtain a non-equilibrium rate of $C_{ne} \simeq 9.7 \times 10^{14} sec^{-1}$. These estimates constitute two limiting values for excitation rates to the 1s-3p state.

Broadening of the line profile at these high densities and higher stages of ionization must be accounted for in the gain calculation. Best estimates for ion broadening due to the Stark effect indicate that the Stark width ($\Delta\lambda \simeq 0.4\text{Å}$) is two orders of magnitude larger than the Doppler width of the line at these conditions.[6,11] The expression

for gain is:

$$G = 10 \log (e) \frac{\lambda^2}{4\pi^2} \frac{A}{\Delta\nu} \left(n_2 - \frac{g_2}{g_1} n_1 \right) \text{ db/cm}, \qquad (10)$$

where λ is the wavelength, A the Einstein coefficient, $\Delta\nu$ the Stark broadened width, n_2 and n_1 the number of atoms in the upper and lower state, respectively, and g_2/g_1 the ratio of their statistical weights. For a pumping time of 10^{-12} seconds and a 1% doped target we calculate a gain of 1 db/cm using an equilibrium cross-section. The gain based on the extreme non-equilibrium cross-section, 4×10^4 db/cm, is unrealistically high because the rate of excitation would saturate on a time scale short compared to 10^{-12} seconds. It is clear, however, that the gain estimate based on equilibrium values is a pessimistic approximation for this process of population inversion.

The case calculated above utilized a slow risetime (10^{-10} second) laser pulse more suitable for efficient ion heating than efficient population inversion. Clearly a faster rise laser pulse ($\leq 10^{-12}$ sec) will lead to higher gain in this transition due to strongly enhanced non-equilibrium effects. Indeed a prepulse sufficient to raise the plasma should achieve a maximum population inversion.

In this calculation we have modeled a mechanism leading to single pass amplification with sufficiently high gain for superradiance from a small volume. Experiments are presently being designed to study the line emission at 128Å under the conditions described.

REFERENCES

1. M. J. Bernstein and G. G. Comisar, J. Appl. Phys. 41, 729 (1970).
2. E. B. Goldman, Numerical Modeling of Laser Produced Plasmas: One-Dimensional Fluid-in-Cell Model, University of Rochester Report No. 6, Laser Energetics Laboratory (1971).
3. W. L. Weise, M. W. Smith, and B. M. Glennon, Atomic Transition Probabilities, NSRDS-NBS4, Vol. 1 (U.S. Gov't Printing Office, Washington, D. C., 1966).
4. J. Dawson and C. Oberman, Phys. Fluids 5, 517 (1962).
5. R. F. Post, Plasma Physics 3, 273 (1961).
6. H. R. Griem, Plasma Spectroscopy (McGraw-Hill, New York, 1964).
7. R. C. Elton, "Atomic Processes", in Methods of Experimental Physics, edited by H. R. Griem and R. H. Lovberg (Academic Press, New York, 1970), Vol. 9A, p. 115.
8. W. Leising, J. McIver, and M. Lubin, Laser Prepulse Studies of Solid Target Vaporization, University of Rochester, Report No. 11, Laser Energetics Laboratory (1972); Bull. Am. Phys. Soc. 16, 1291 (1971).
9. R. C. Elton, Determination of Electron Temperatures Between 50 eV and 100 KeV from X-ray Continuum Radiation in Plasmas, Naval Research Laboratory, NRL Report 6738, Washington, D. C. (1968).
10. M. J. Seaton, "The Theory of Excitation and Ionization by Electron Impact", in Atomic and Molecular Processes, edited by D.R. Bates (Academic Press, New York, 1962), p. 374.
11. D. D. Burgess, B. C. Fawcett, and N. J. Peacock, Proc. Phys. Soc. 92, 805 (1967).

FIGURE CAPTIONS

Fig. 1 Development of laser heated impurity doped plasma sphere, showing the density (a) and electron temperature (b) at various times. Incident laser energy 265 joules at $\lambda = 1.06\mu m$ delivered in 10^{-10} seconds.

Fig. 2 Time history of line radiation showing the power (a) and energy (b) in each line. Impurity doping concentration is 1%. Rise time of each line is less than 10^{-11} seconds.

Fig. 3 Energy level diagram of OVII. The transition of interest for a population inversion is 2s-3p.

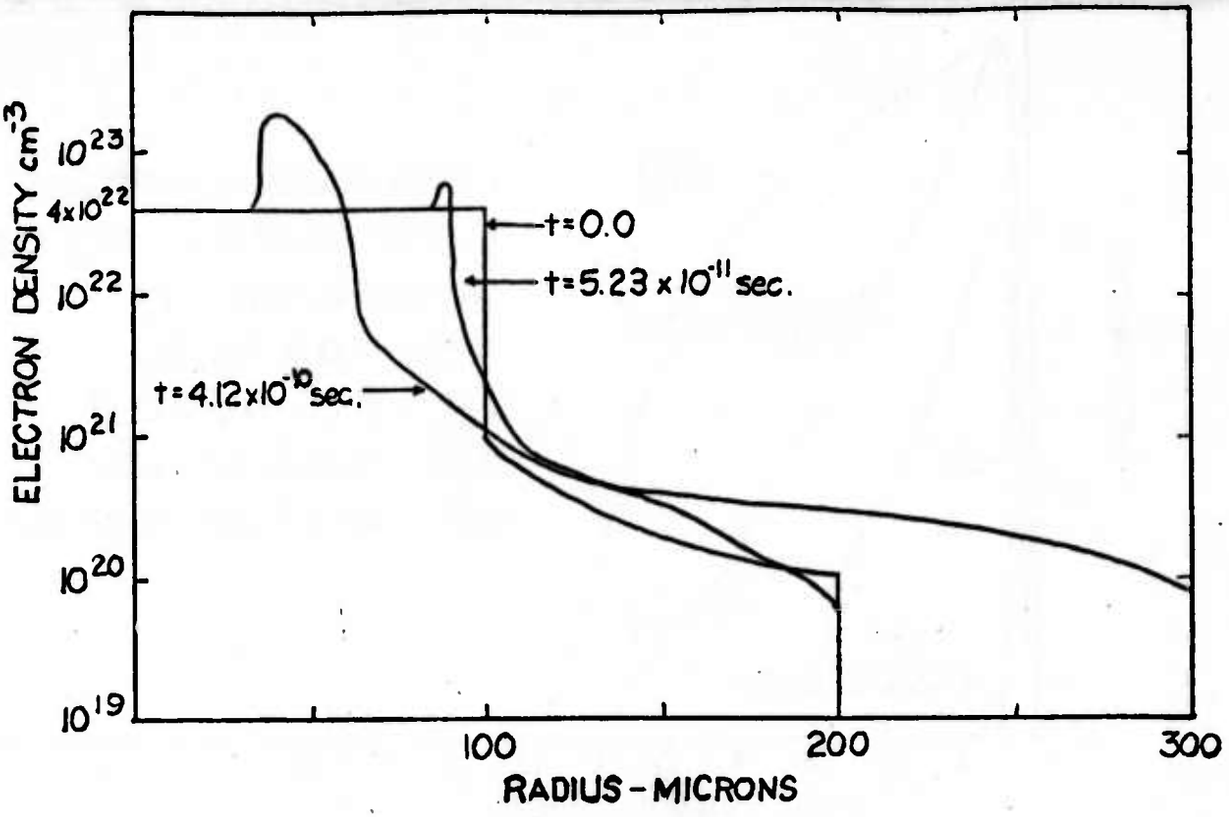
ELECTRON DENSITY cm^{-3}
10^{23}
4×10^{22}
10^{22}
10^{21}
10^{20}
10^{19}
t=0.0
t=5.23 x 10^{-11} sec.
t=4.12x10^{-10}sec.
100
200
300
RADIUS - MICRONS

(a)

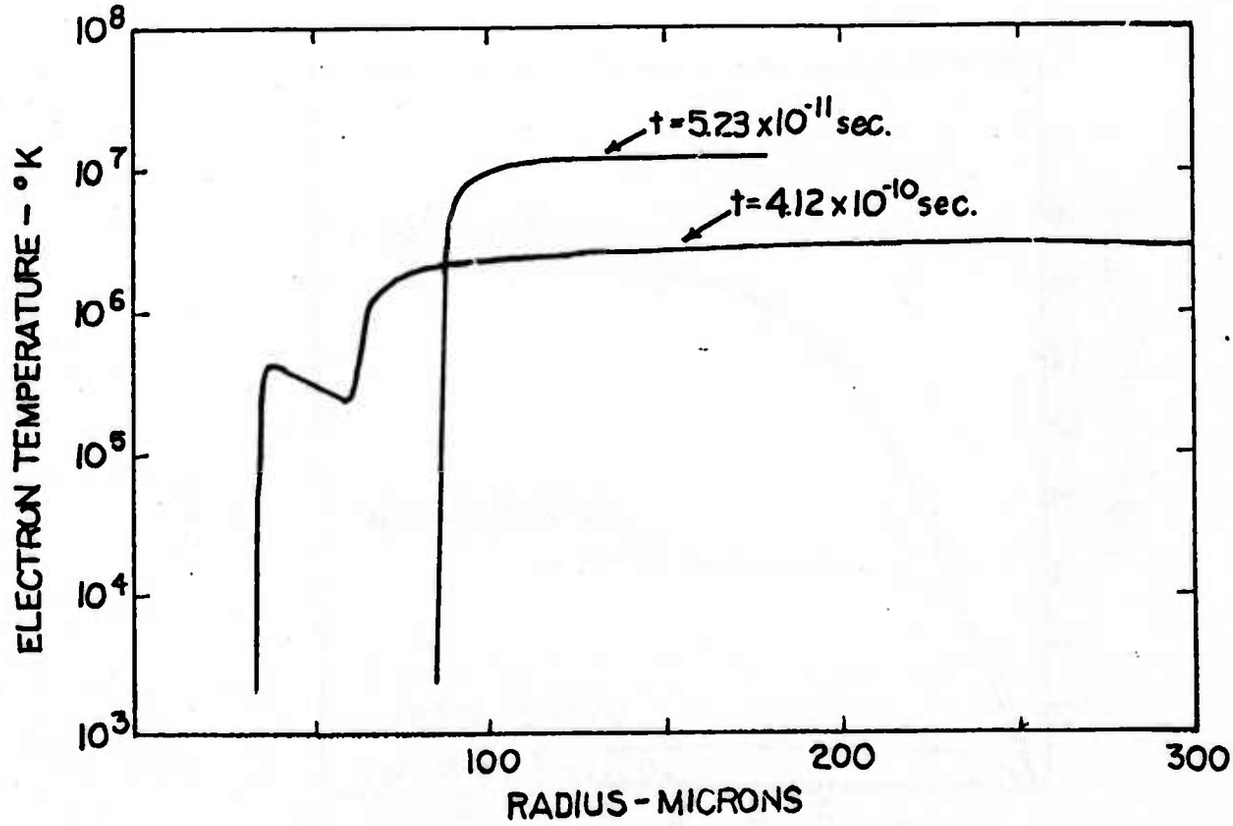
ELECTRON TEMPERATURE - °K
10^{8}
10^{7}
10^{6}
10^{5}
10^{4}
10^{3}
t=5.23 x10^{-11}sec.
t=4.12 x10^{-10}sec.
100
200
300
RADIUS - MICRONS

(b)

Fig. 1

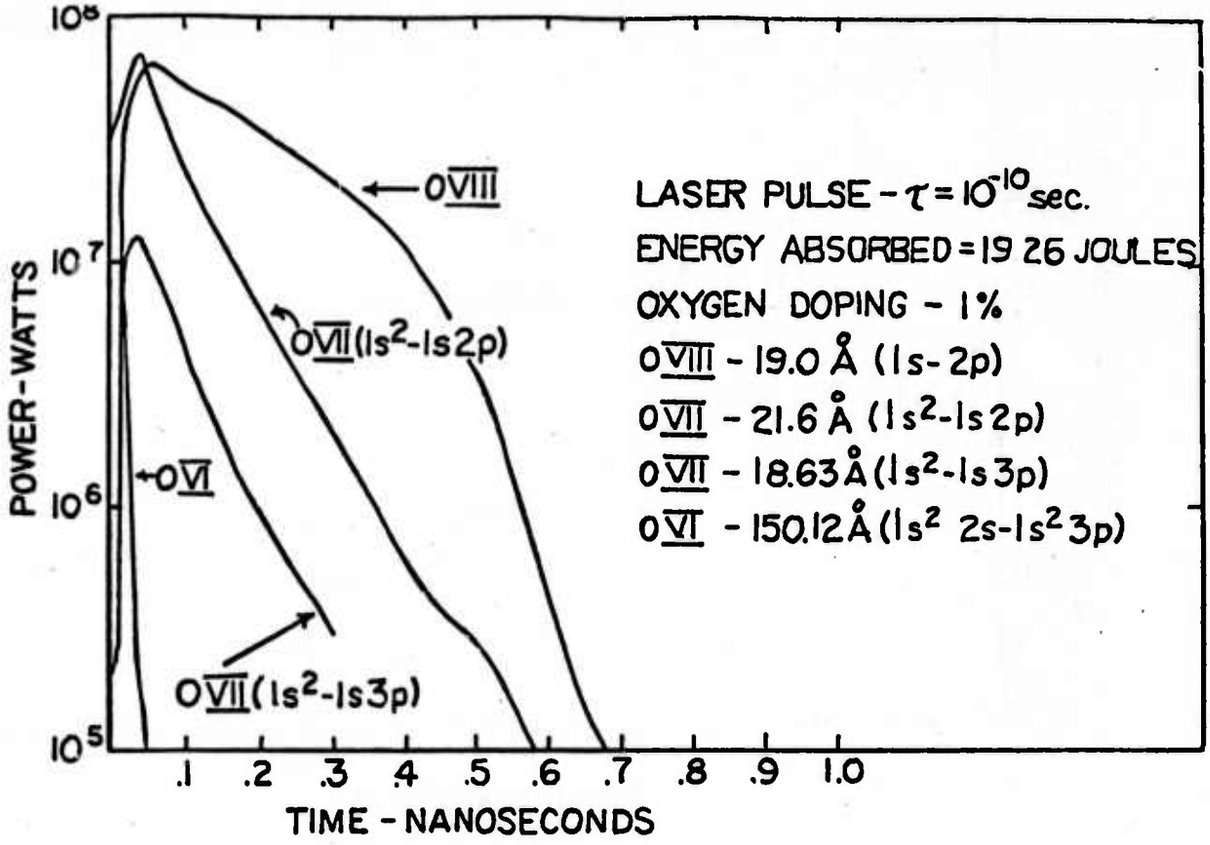
POWER-WATTS
TIME - NANOSECONDS
OVIII
OVII(1s²-1s2p)
OVI
OVII(1s²-1s3p)
LASER PULSE - τ = 10⁻¹⁰ sec.
ENERGY ABSORBED = 19 26 JOULES
OXYGEN DOPING - 1%
OVIII - 19.0 Å (1s-2p)
OVII - 21.6 Å (1s²-1s2p)
OVII - 18.63 Å (1s²-1s3p)
OVI - 150.12 Å (1s² 2s-1s²3p)

(a)

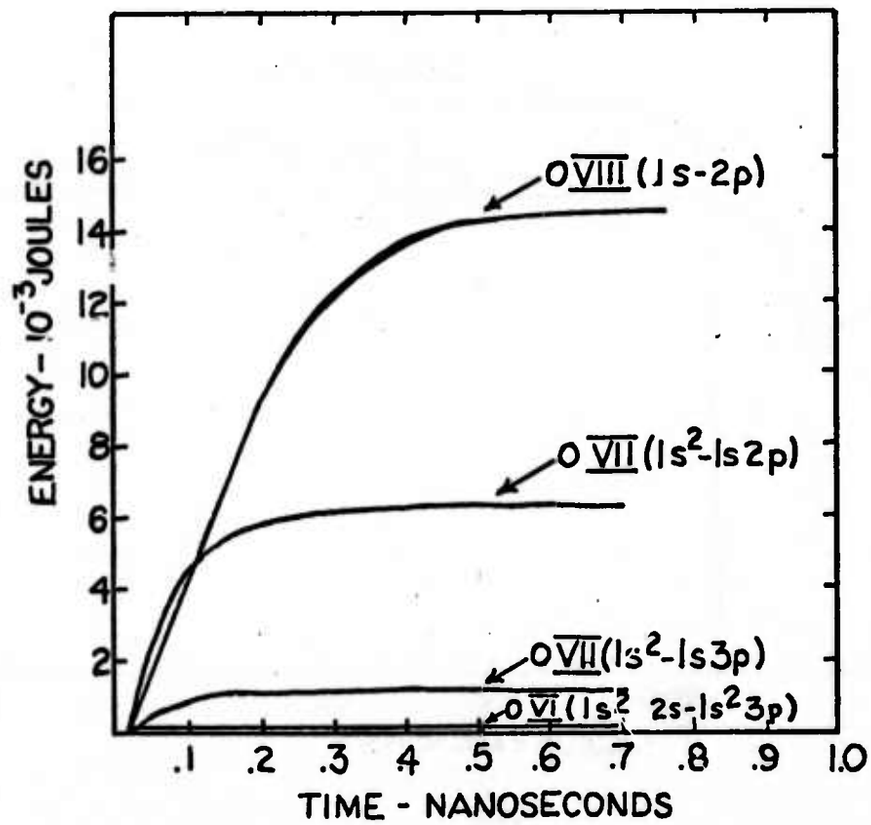
ENERGY - 10⁻³ JOULES
TIME - NANOSECONDS
OVIII (1s-2p)
OVII (1s²-1s2p)
OVII(1s²-1s3p)
OVI (1s² 2s-1s²3p)

(b)

Fig. 2

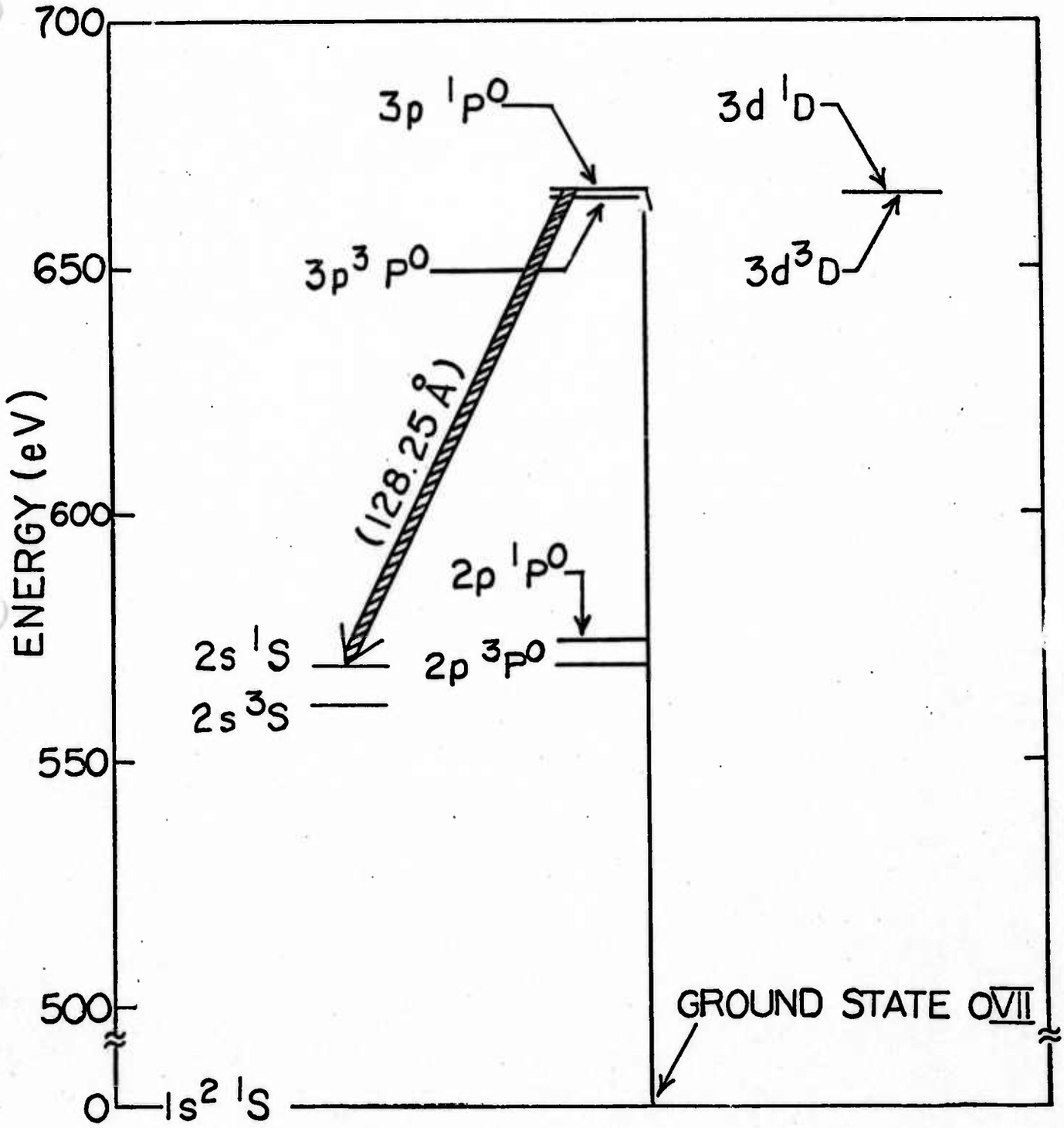
700
650
600
550
500
0
ENERGY (eV)
3p ¹P⁰
3d ¹D
3p³ P⁰
3d³D
(128.25 Å)
2p ¹P⁰
2s ¹S
2p ³P⁰
2s ³S
GROUND STATE OVII
1s² ¹S

Fig. 3

SPATIAL RESOLUTION OF LASER PRODUCED PLASMAS WITH X-RAY CRYSTALS

Report No. 28

by

B. Yaakobi, T. Bristow, and A. Hauer

March 1975

This work has been supported by ARPA Grant N0014-67-A-0398-0017, ARPA Grants DAHC04-74-G-0236, DAHC04-~~71-C-0046~~ and ONR Grant N0014-72-C-0046.

A B S T R A C T

X-ray spectra taken with good quality flat crystals can yield spatial resolution of small plasma sources at the expense of spectral resolution. 40μm spatial resolution of a laser-produced aluminum plasma was obtained using lines of wavelength ~6Å.

Pinhole x-ray photographs of laser-produced plasmas are currently employed as a fruitful means of obtaining information on the hydrodynamic behavior of pellets irradiated by lasers[1],[2]. In the following we show that plane crystals directly illuminated by the plasma source can yield similar results for various wavelengths. This richer information is obtained without slits or pinholes, provided the following conditions are satisfied: (a) the crystal has a small mosaic spread, (b) well separated spectral lines are employed, of small intrinsic width, and (c) the spectrometer is placed sufficiently far away from the source. All these conditions can be readily met and result in a spatial resolution of 40μm or better.

As an illustration, we measured the spectrum in the range (5-8)Å emitted from an aluminum plane target irradiated by a neodymium glass laser [3]. The crystal used was rubidium acid phthalate (from Quartz Products Corp.) of 2d-spacing 26.12Å. The pulse parameters were: energy 4J, pulsewidth 0.2 nsec., focal spot diameter ~100μm. We place the crystal in two different positions as shown in fig. 1 (a) and (b). Portions of the resulting spectra are shown in fig. 2. Typically, the lines have one wing which rises much faster than the other and which appears on the side which receives radiation from the plasma layer closest to the target surface. Clearly, what we get is not the spectral shape of the lines but rather the spatial variation of the integrated line intensity. Ind , by following parallel rays from different points of the source we can easily see that the width of a spectral line in a plane perpendicular to the ays simply equals the source size, and the asymmetry of the lines in fig. 2 is a reflection of the one-directional expansion of the plasma created at a plane target. The comparison of different spectral lines can provide insight into laser produced plasma

sources (plane or spherical) not available from pinhole photographs or non-focusing spectrographs which do not conform to the conditions listed above (i.e., spatially resolved temperature and density determinations).

We have also included in fig. 2 an x-ray pinhole image of a plane target illuminated by a 10^{13}W/cm^2 laser of 10 nanosecond duration [1]. The similarity in the shapes of the curves obtained by the two different methods is evident.

We now discuss in more detail the conditions for spatial resolution. The mosaic spread of crystals of the acid phtalates family is known to be very small [4]; for the line of fig. 2 it is about 0.3 arc minutes, which is equivalent in our case to a broadening of 2×10^{-3}Å. A good choice of lines for this work is some intermediate member (or members) of a resonance series in order to minimize both the Stark broadening and the broadening due to self-absorption. Also, these two broadening mechanisms become less significant for the same transitions as one goes to higher-Z materials. Near the critical layer $N_e \sim 10^{21}$cm^{-3} and it can be shown that the Stark widths [5] of the first 2-3 members are smaller than their Doppler widths whereas the reverse is true for the higher members. The additional broadening due to self-absorption (by a factor $(\ln\tau_o)^{\frac{1}{2}}$) is not very large even for the first member of the two series shown in fig. 2, for which the optical depth at line center τ_o is estimated to be of order 10^2; it is certainly insignificant for the higher members. For an ion temperature 0.5keV [6] the Doppler width of these lines is 0.002Å and this translates, in the geometry of fig. 1, into a width 40μm at the film. This figure is thus representative of the achievable spatial resolution.

Higher spatial resolution would require reduction in the source-spectrometer distance. Another consideration in seeking good spatial resolution is the choice of crystal. From the Bragg condition, $2d\sin\theta=\lambda$, it follows that larger 2d spacings minimize the angular spread diffracted at a given wavelength. Further, at a given wavelength a larger 2d spacing requires smaller Bragg angles which reduces the width of the rocking curve [4].

As the source-crystal distance is increased, so does the wavelength dispersion, but the width on the film corresponding to the source size remains the same. Therefore close distances are favorable for spatial resolution (until neighboring lines start to overlap) whereas long distances are favorable for spectral resolution. Closer distances are also favorable for energy per unit area arriving at the film (although the total intensity of a line remains constant).

Another interesting feature of the present idea is that one can choose to have good spectral resolution on the short or the long wavelength side of a given line by going from position (a) to (b) in fig. 1.

Of course, a slit in front of the spectrometer can give simultaneous spectral and spatial resolutions in mutually perpendicular directions. However, the proper choice of lines and geometry allows the trade-off of spatial resolution against the (co-directional) spectral resolution in a much simpler setup.

ACKNOWLEDGEMENT

This work has been supported by ARPA Grant N0014-67-A-0398-0017, ARPA Grants DAHC04-74-G-0236, DAHC04-~~71-C-0046~~ and ONR Grant N0014-72-C-0046.

REFERENCES

[1] T.P. Donaldson, R.J. Hutcheon, and M.H. Key, J. Phys. B. 6, (1973) 1525; M.H. Key, K. Eidman, E. Dorn, and R. Sigel, Phys. Lett. 48A (1974) 121.

[2] P.M. Campbell, G.C. Charatis, and G.R. Montry, Phys. Rev. Lett. 34, (1975) 74.

[3] T.C. Bristow, M.J. Lubin, J.M. Forsyth, E.B. Goldman, and J.M. Soures, Optics Comm. 5 (1972) 315.

[4] A.J. Burck, D.M. Barrus, and R.L. Blake, Astrophys. Journal 191, (1974) 533.

[5] H.R. Griem "Spectral Line Broadening by Plasmas" (Academic Press, New York, 1974).

[6] See for example: K.G. Whitney and J. Davis, J. of Appl. Phys. 45, (1974) 5294; Steady state corona model gives a temperature slightly higher than 0.5keV when these lines are at maximum but the ion temperature lags behind and is somewhat smaller.

FIGURE CAPTIONS

1. Geometrical arrangement of the measurement. The crystal was placed in either position (a) or (b). θ is the Bragg angle for the longest (in a) or the shortest (in b) wavelength in the range observed. In each case the source-crystal and the crystal film distances are about 5cm.

2. (a) and (b), part of the spectra obtained for the corresponding positions in Fig. 1 as seen through a 25 m thick beryllium window, (c) an x-ray pinhole image of a plane target from ref. 1. The wavelength scale refers to (b) and is slightly expanded for (a). The lines are: Al XII: (t) 1s-4p, (u) 1s-5p, (v) 1s-6p; Al XIII: (w) 1s-3p. The difference in the background continuum in (a) and (b) is instrumental and is irrelevant to the present discussion.

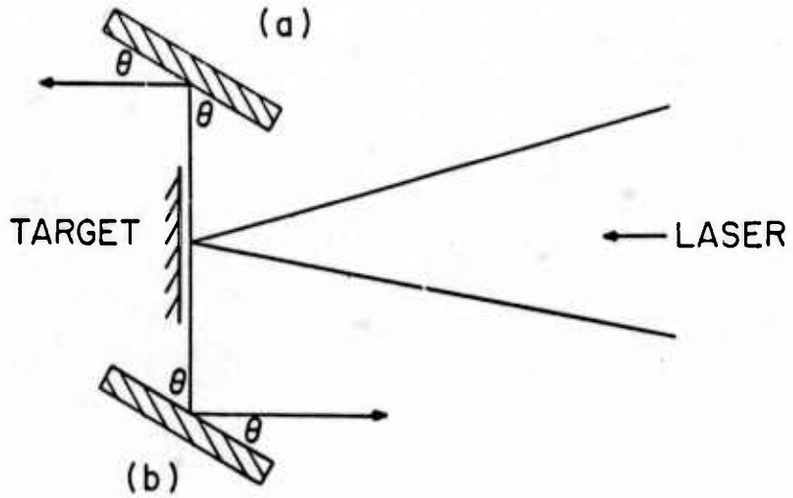

Figure 1

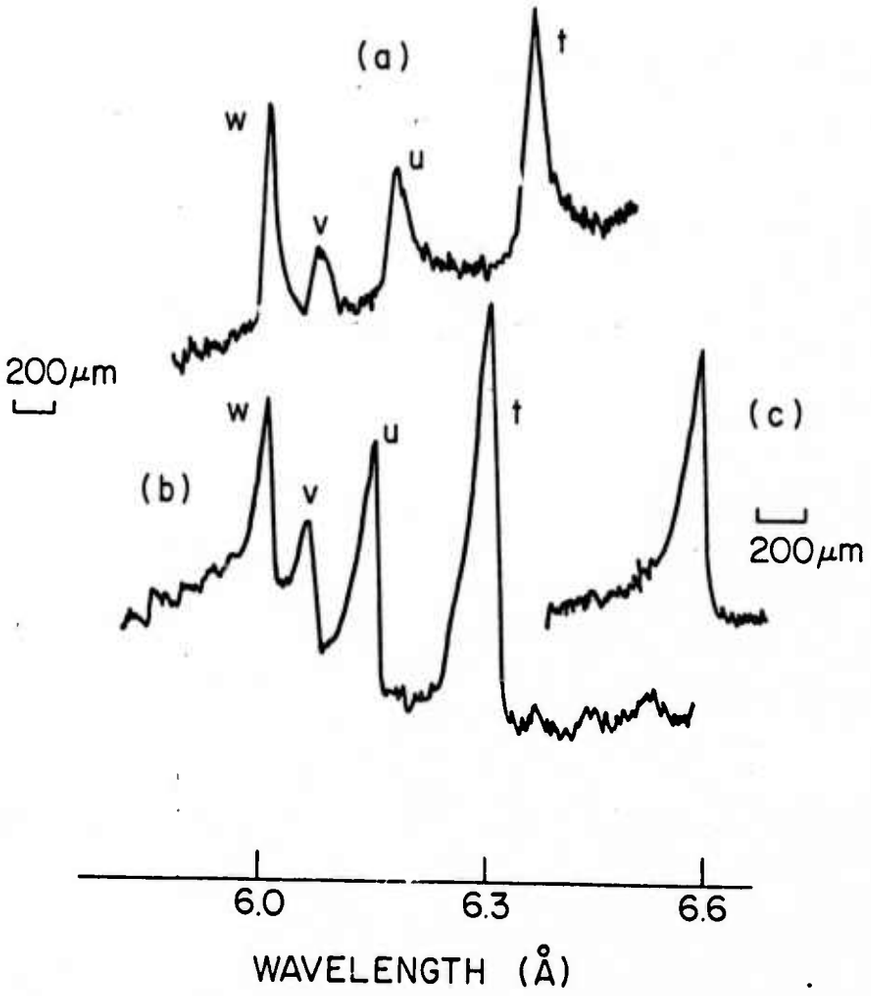

Figure 2

"Spatially Resolved and Stark-Broadened X-ray Lines from Laser Imploded Targets"

Report No. 37

B. Yaakobi and A. Nee
University of Rochester

ACKNOWLEDGEMENT

The research reported on herein was supported by the following principal sponsors:

Exxon Research & Engineering Company
General Electric Company
Northeast Utilities Service Company
Empire State Electric Energy Research Company
University of Rochester

Others contributing to the efforts of the work in the Laboratory for Laser Energetics include:

U.S. National Science Foundation
New York State Atomic & Space Development Authority
New York State Science & Technology Foundation
U.S. Air Force Office of Scientific Research
Advanced Research Projects Agency

Such support does not imply endorsement of the content by any of the above parties.

April 1976

ABSTRACT

We report the first observation of spatially resolved x-ray lines from laser-irradiated spherical targets. The lines are found to emanate mainly from inside the critical layer but the density they all indicate is not much higher than critical. These results are relevant to the study of heat conductivity and the laser ponderomotive force.

The transfer of absorbed laser energy into super-critical layers of an irradiated target has been shown recently to be very complicated. In particular, heat flow may be inhibited by magnetic fields[1] or be non-classical[2] and the density profile may be modified by the laser ponderomotive force.[3] We show here that x-ray line spectroscopy with spatial resolution can be a very useful tool for studying such effects. The targets used in these experiments, glass spherical shells, contain a variety of species (silicon, oxygen, sodium, magnesium) and the comparison of their spectra forms the basis for the present method. Additional information was gained by comparing such measurements with the emission at twice the laser frequency, which was spatially[4] and temporally[5] resolved. The results indicate a plateau (or "upper shelf") in the density profile extending roughly 20-30μm inwards from the critical layer (see Fig. 2). The failure to observe densities substantially higher than critical can be due to reduced or inhibited heat conductivity.

A four-beam glass:Nd laser system producing pulses of length 0.2-0.4 nsec was used to illuminate glass spherical shells of diameter about 90μm and wall thickness 1μm. The fill gas was neon at about ten atmosphere pressure. Absorbed energy from all four beams ranged from 5 to 10J. Incident power was 0.6-0.8 TW and power density $(2\text{-}3)10^{15}$ W/cm^2. A more detailed description of the laser system and diagnostic methods employed can be found in the literature.[6] Spectra were analyzed by a flat Thalium Acid Phthalate crystal and recorded on a calibrated no-screen film. A slit of width 14μm was placed between the target and the (non-focusing) spectrometer so as to achieve linear magnification 7 and spatial resolution 16μm in a direction perpendicular to that of the spectral resolution.

The usefulness of x-ray spectra lies in the fact that lines from a given species will be emitted mostly when the temperature lies in a certain limited range. By spatially resolving the strong resonance lines in helium-like and hydrogen-like ions of the glass elements we can find the target regions where these species emit strongly. Using the spatially-integrated spectra we can then estimate the temperature and density at these respective regions. Figs. 1 and 2 show that the emission from the various species come from well-defined thin shells which are slightly displaced with respect to each other. This kind of characteristic behavior is expected, even though the spectra are time-integrated. Thermal energy flows from the critical layer into the expanding glass shell in the form of a sharp heat step function of temperature $\sim$1 keV.[7] Lines from light elements ($Z \lesssim 12$) are thus emitted predominantly within the narrow heat front. Even as it moves in, the region emitting a given spectral line will approximately retain its temperature. Unless absorbed energy is too high, the heat front movement is arrested by a rarefaction wave (ablation) and this gives rise to a quasi-stationary spatial profile. Since x-ray emission is weighted by the density, we expect most of the line radiation to come from the conduction layer and be sensitive to the heat conductivity and the density profile behind the critical layer. Fig. 1 shows that sodium resonance lines come from inside the critical layer. To see this we note that the critical layer (as determined by the emission at twice the laser frequency) was found to spend most of the pulse duration at the position of its maximum excursion.[5] Also, it is the outer edge of the 2ω emission contour which marks this position.[4] We see that species of lower charge are excited at smaller radii which is evidence of an inwardly decreasing temperature. The Abel inversion procedure required to derive Fig. 2 from results such as in Fig. 1

assumed the plasma to be cylindrical. This was found to be the case when imaging the target with an x-ray pinhole camera, in and perpendicular to the plane of the laser beams.

We now turn to the spatially integrated spectra and give only a few examples of how they were used to derive temperature and density estimates. The temperature from the silicon spectrum (Fig. 3) was estimated using three intensity ratios: (a) between the resonance lines of Si^{+13} and Si^{+12}, (b) between the $1s^2$-1s3p and $1s^2$-1s2p lines of Si^{+12}, and (c) between the resonance line of Si^{+12} and the nearby group of dielectronic satellites.[8] We assume a steady state corona model[9] in (a) but no such assumption is required in (b) or (c). Two conditions are required for the steady state corona model to be valid: $N_e < 10^{16} z^7 (kT/I_z)^{\frac{1}{2}}$ where I_z is the ionization energy; also, the ionization time $\tau \sim 10^8 z^3/N_e$ (assuming $I_z/kT=2.5$) should be shorter than plasma characteristic times. Density estimates below show the first condition to be satisfied here. Ionization times vary from about 50psec to 200psec when z increases from 8 to 13. The distance ions travel during this time is not much larger than the resolution length in Fig. 2. We conclude that steady state is marginally applicable, especially since the ratio (a) is extremely sensitive to T. In fact, if we solve the coupled equations which describe the steady state corona model for the silicon ions we find that Si^{+12} attains its maximum abundance at 0.8 keV and Si^{+13} at 1 keV; the observed ratio (a) is that predicted by this model for T=0.9 keV. A similar situation is found for the other species. The ratios (b) and (c) are inconsistent with this result and can only be understood if resonance lines are attenuated by absorption. If we assume the resonance line of Si^{+12} to be attenuated by a factor 3, then <u>both</u> ratios (b) and (c) give approximately T=0.9 keV. This attenuation can be shown to be consistent[10] with the

product of density and plasma shell thickness as discussed below. A reduction by a factor 3 in the intensity ratio (a) results in a reduction of only 20% in T. Actually, the resonance line of Si^{+13} should also be slightly absorbed and the error could be somewhat smaller. Comparing these and similar results we conclude that the temperature drops from about 0.9 keV around the critical layer (peak radiation of silicon) to about 150eV (peak radiation of oxygen) over a distance which we can only roughly estimate as 20-30μm.

The density is estimated by two methods. First, the intensity ratio between the resonance line $1s^2$-$1s2p\,^1P$ and the intercombination line $1s^2$-$1s2p\,^3P$ is weakly dependent on temperature and increases linearly with N_e when the quenching rate of the metastable state is intermediate to the radiative decay rates of the singlet and triplet states.[11] Accounting for self-absorption of the resonance line as above gives an observed ratio of about 10 for silicon (Fig. 3, insert). The corresponding density is about equal to the critical density $N_c=10^{21}cm^{-3}$, in agreement with Fig. 2. We have assumed here T=0.9 keV; varying T by a factor 2 will only change the derived value of N_e by about 30%. The intercombination lines in the lower Z spectra should be weaker even for the same density and were hardly discernible in our spectra.

We finally estimate the density from the Stark widths of the last resolvable lines in the various resonance series. These lines would be broadened predominantly by ions which can be treated in the quasi-static approximation and the high lying levels would be hydrogenic (degenerate) even for the helium-like ions. We note that for a given N_e the broadening due to ions decreases with z like $z^{-2/3}$ whereas the broadening due to electrons decreases like z^{-3} (assuming a constant T/z^2). We forgo at this stage accurate profile calculations and seek only the line half-

widths. The quasi-static Holtsmark broadening in angular frequency units of a transition from level n_i to n_f in an ion of charge z due to ions of density N_p and charge z_p is[12] $\Delta\omega=(12z_p h/zm)(n_i^2-n_f^2)N_o^{2/3}$. To account for ion-ion correlation we divide this expression by the ratio of the line width due to a Holtsmark distribution and that due to a correlated distribution.[13] The appropriate value of z in these calculations enter only in the Holtsmark "normal" field[13] and in the Debye length. For oxygen, this length turns out to be slightly smaller than the interparticle distance and we must extrapolate Hooper's results.[13] The same procedure in equivalent low-z cases[12] has a precision better than a factor 2, but the precision for the spectra under discussion is not really known. The silicon lines (Fig. 3) are broadened mostly due to the finite size of the emitting plasma. Even for the last resolvable line of the $1s^2$-1snp series (i.e., n=5) we see no further broadening with respect to earlier series members and this translates into $N_e<<5N_c$. Oxygen lines from high-lying levels (more sensitive to the Stark effect because of the lower z) do show a significant Stark broadening (Fig. 4). Assuming Voigt profiles and eliminating the instrumental broadening (given by the narrowest line in the spectrum) we obtain for the lines 1s-np (n=5,6,7) the widths 16,19 and 31 mÅ; the last width was derived from the long-wavelength wing of the line. The first and third of these give a density $N_e\sim N_c$; the 1s-6p line appears too narrow for this density, probably because of its unshifted Stark component. The highest transition in sodium which is clearly seen is $1s^2$-1s4p which barely shows a broadening beyond the instrumental width. This translates into $N_e<<6N_c$.

Two important conclusions seem to follow from these measurements. First, by comparing the density obtained by the various species and from Figs. 1 and 2, it follows that a region of thickness $\lesssim$20-30μm behind

the critical layer has a density confined to the approximate range (1-2)N_c. This could be an observation of the "upper shelf" seen in particle simulations.[3] It follows from here that the pressure in the conduction region increases outwards which resembles the choked flow through a nozzle (the sonic point would be close to the critical layer). Second, the penetration depth of the heat front from the critical layer inwards is given approximately by[7] $d \sim K/vN_e$ where K is the heat conductivity and v the ion thermal speed. For $d \sim 20\mu m$ one calculates a value of N_e an order of magnitude larger than actually measured. This can be explained by a coefficient K an order of magnitude smaller than classical which prevents the heat front from penetrating into the denser part of the expanded glass shell.

ACKNOWLEDGEMENT

We are grateful to L.M. Goldman, T.C. Bristow, J. Hoose, and S. Letzring for fruitful discussions and invaluable assistance.
This work was partially supported by the Laser Fusion Feasibility Project in the Laboratory for Laser Energetics at the University of Rochester, and ARPA Grant No. DAHC04-71-C-0046.

REFERENCES

1. B.H. Ripin, et al., Phys. Rev. Lett. 34, 1313 (1975).
2. R.C. Malone, R.L. McCrory and R.L. Morse, Phys. Rev. Lett. 34, 721 (1975); W.C. Mead, W.L. Kruer, J.D. Lindl and H.D. Shay, Lawrence Livermore Lab. Preprint 77, 139 (1975).
3. J.M. Kindel, Bull. Amer. Phys. Soc. 20, 1230 (1975); D.W. Forslund et al., Phys. Rev. A11, 679 (1975), ibid, 36, 35 (1976); J.S. DeGroot and J.E. Tull, Phys. Fluids 18, 672 (1975).
4. S. Jackel, J. Albritton, and E.B. Goldman, Phys. Rev. Lett. 35, 514 (1975).
5. S. Jackel, J. Albritton, E.B. Goldman, and S. Letzring, Bull. Amer. Phys. Soc. 20, 1335 (1975).
6. J.Soures, L.M. Goldman, and M. Lubin, Nuclear Fusion 13, 829 (1973).
7. K.A. Brueckner and S. Jorna, Rev. Mod. Phys. 46, 325 (1974); K.A. Brueckner, R.A. Campbell and R.A. Grandey, Nuc. Fusion 15, 471 (1975).
8. A.H. Gabriel, Mon. Not. Roy. Astron. Soc. 160, 99 (1972); C.P. Bhalla, A.H. Gabriel, and L.P. Presnyakov, ibid, 172, 359 (1975).
9. H.R. Griem, "Plasma Spectroscopy" (McGraw-Hill, New York, 1964) ch. 6.
10. A.G. Hearn, Proc. Phys. Soc. (London) 81, 648 (1963).
11. A.H. Gabriel and C. Jordan, in Case Studies in Atomic Collision Physics 2, ed. E.W. McDaniel and M.R.C. McDowell (North-Holland, Amsterdam, 1972), ch. 4.
12. H.R. Griem, Spectral Line Broadening by Plasmas (Academic Press, New York, 1975), p. 8.
13. C.F. Hooper, Phys. Rev. 165, 215 (1968); J.T. O'Brien and C.F. Hooper, Phys. Rev.A5, 867 (1972).

FIGURE CAPTIONS

Fig. 1 Spatially resolved emissions of: 2ω, twice the laser frequency[4] (resolution 10μm); the resonance lines of Na^{+9} and Na^{+10} and a band of the continuum around 10.5Å (resolution 16μm). All intensities are in arbitrary units. Also shown are the original target position and the maximum excursion of the critical layer. The continuum was not employed in the present study.

Fig. 2 Spatial distribution of some sodium and silicon resonance lines obtained by applying an Abel inversion program to results such as in Fig. 1. The plasma was assumed cylindrical. The inversion results inside the emitting shell are uncertain. The profile for Si^{+12} is similar to that of Si^{+13}.

Fig. 3 Part of the silicon x-ray spectrum. The sharp cut on the right corresponds to the edge of the crystal. Note the well-resolved dielectronic satellites (marked s) and the new satellite at (5.561 ± 0.008)Å. Insert: R - the resonance line $1s^2$-$1s2p\,^1P$ at 6.65Å, I.C. - the intercombination line $1s^2$-$1s2p\,^3P$ at 6.69Å, S - dielectronic satellites (designated[8] j, k, l) around 6.737Å.

Fig. 4 The last few resolvable lines of H-like oxygen.

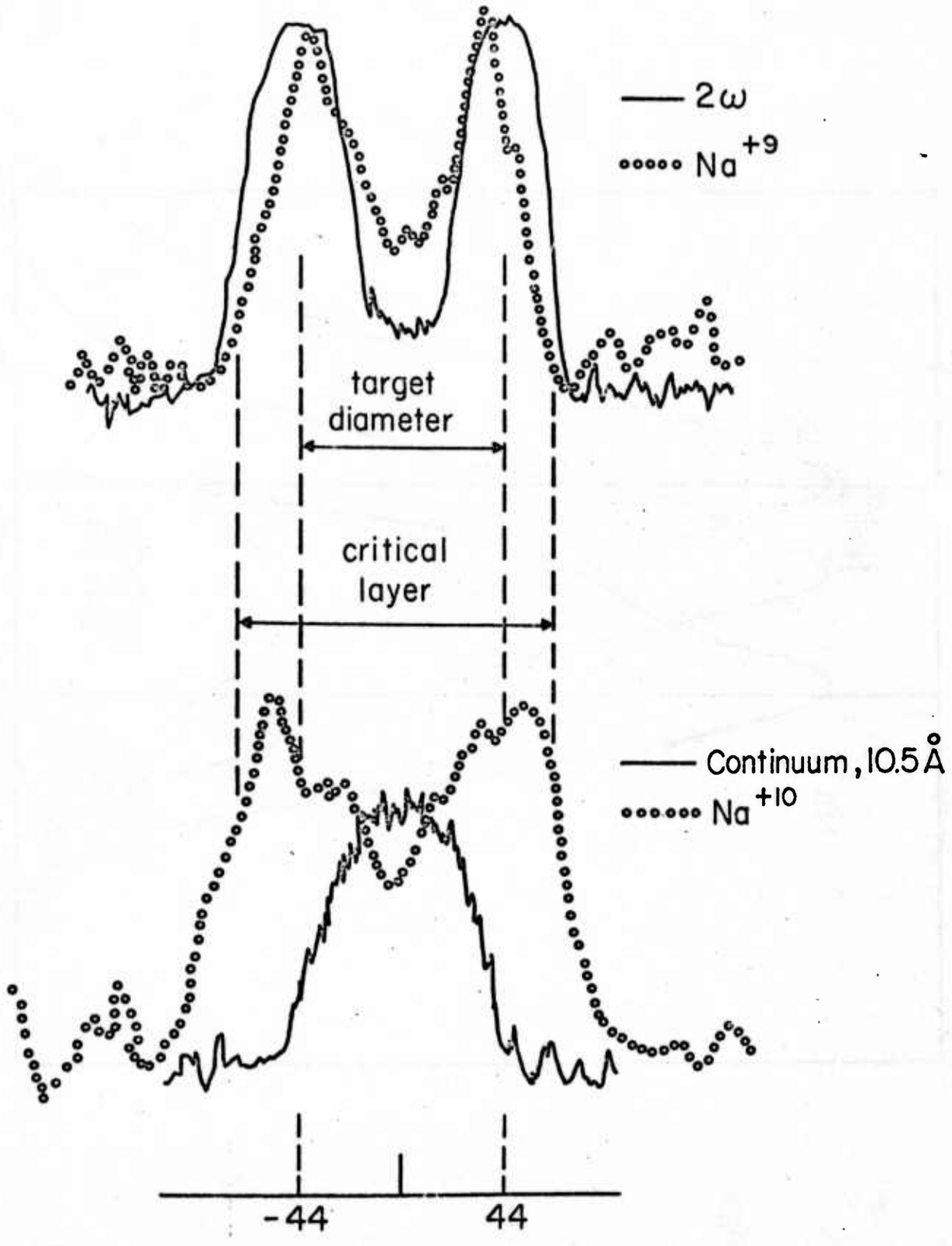

Fig. 1

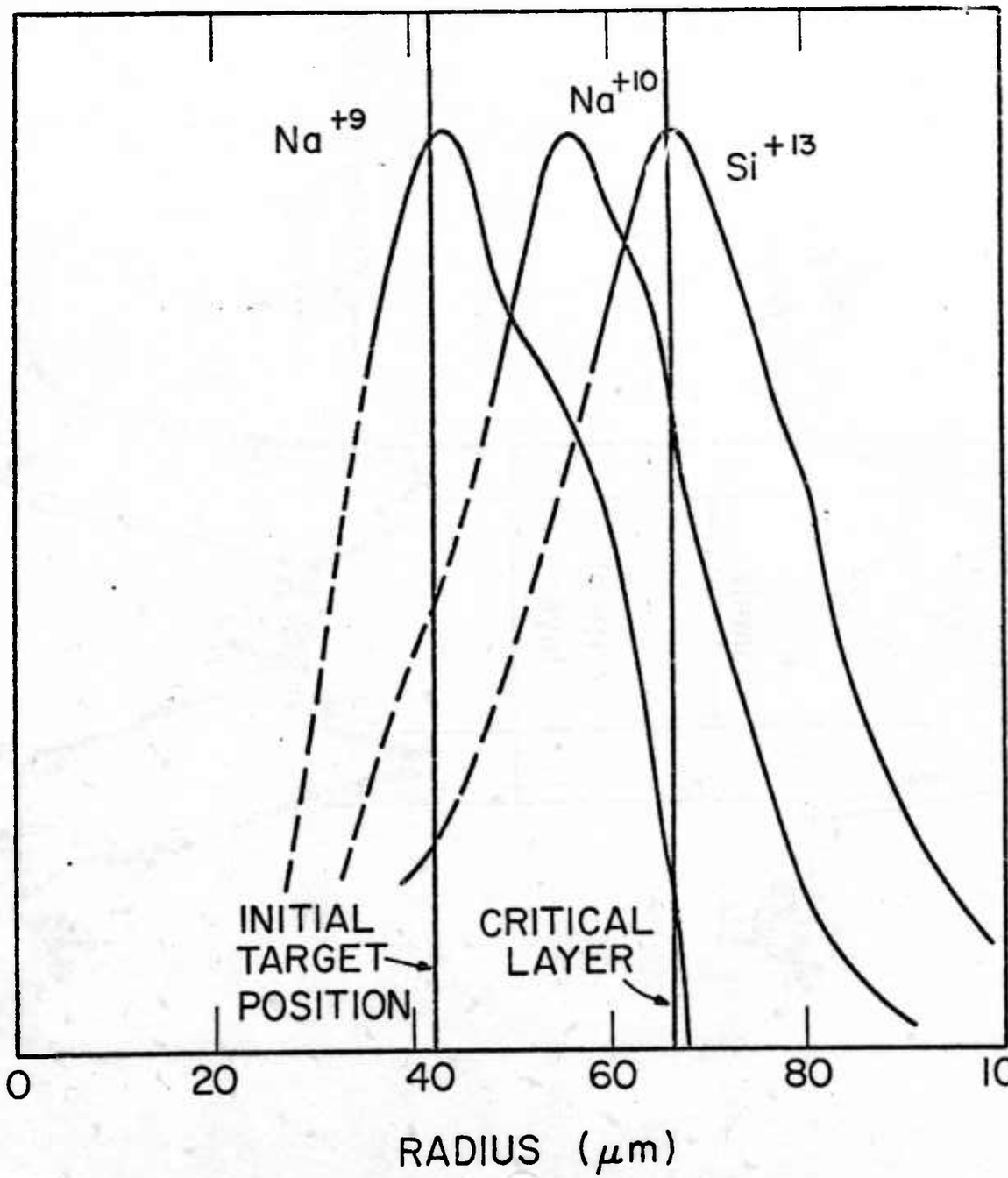
Na+9
Na+10
Si+13
INITIAL TARGET POSITION
CRITICAL LAYER
0
20
40
60
80
100
RADIUS (μm)

Fig. 2

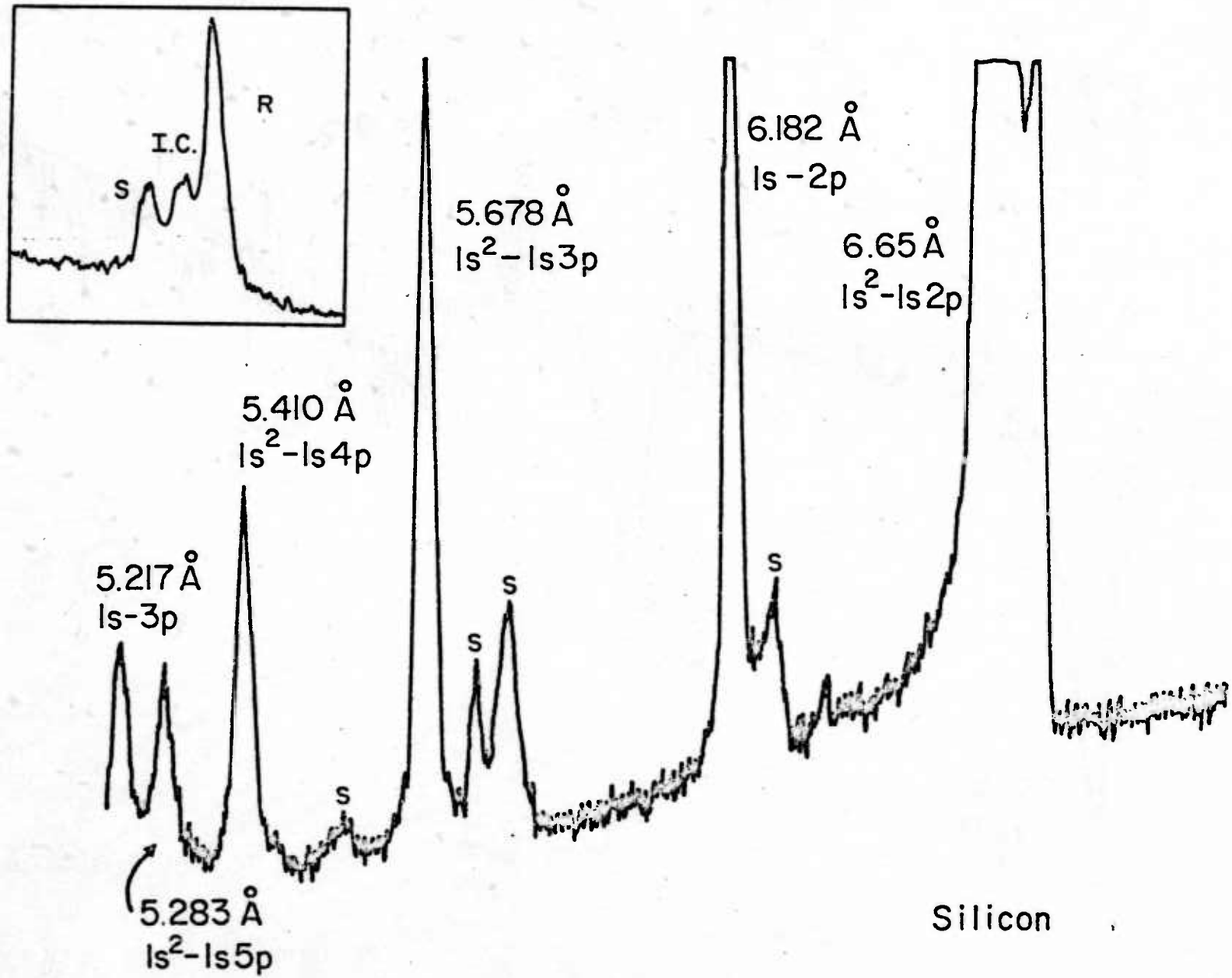
R
I.C.
S
5.678 Å
$1s^2-1s3p$
6.182 Å
$1s-2p$
6.65 Å
$1s^2-1s2p$
5.410 Å
$1s^2-1s4p$
5.217 Å
$1s-3p$
S
S
S
S
5.283 Å
$1s^2-1s5p$
Silicon

Fig. 3

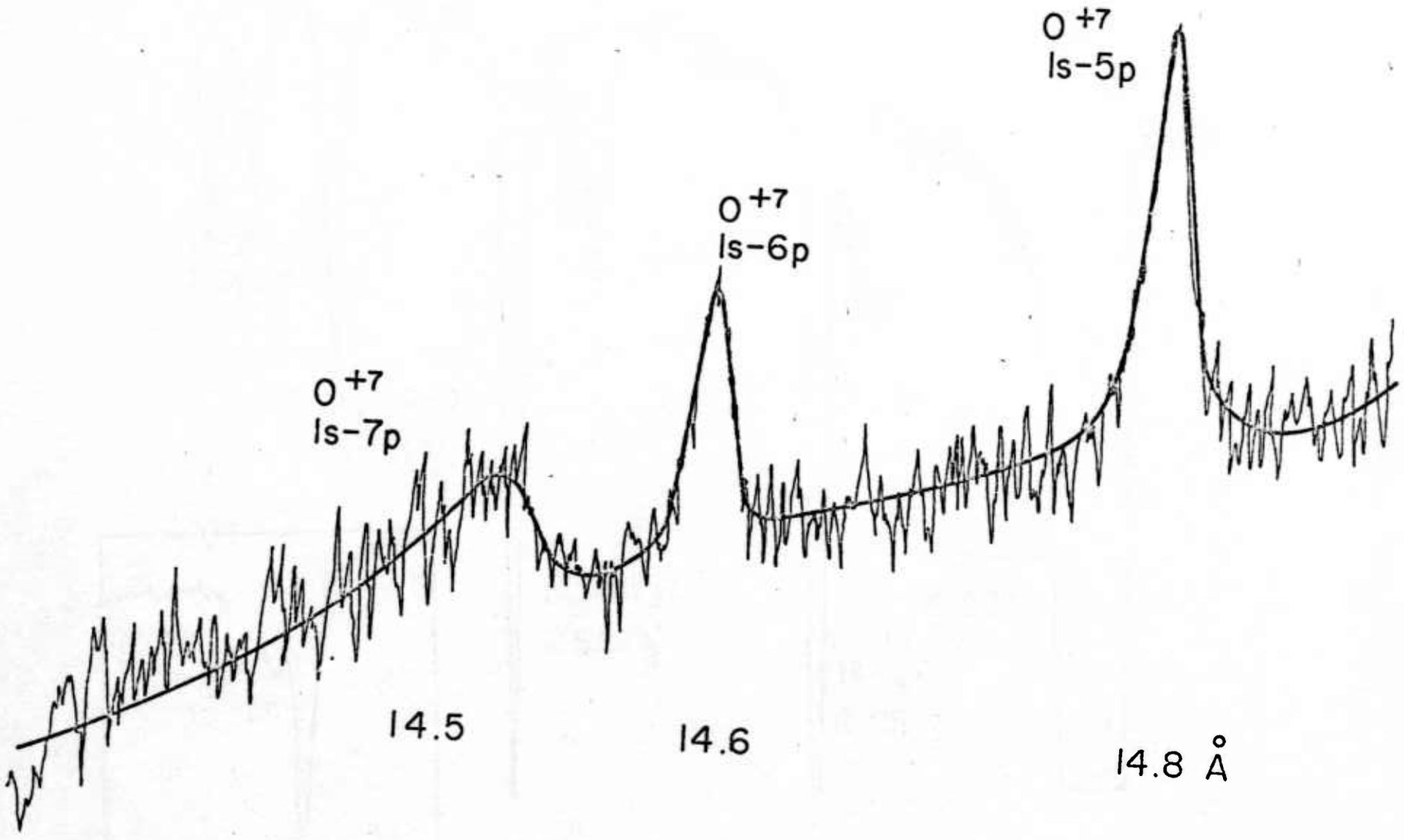

Fig. 4

"Soft X-Ray Population Inversion by Resonant Photoexcitation
In Multi Component Laser Plasmas"

Report No. 41

V. A. Bhagavatula
University of Rochester

ACKNOWLEDGEMENT

The research reported on herein was supported by the following principal sponsors:

Exxon Research & Engineering Company
General Electric Company
Northeast Utilities Service Company
Empire State Electric Energy Research Company
University of Rochester

Others contributing to the efforts of the work in the Laboratory for Laser Energetics include:

U.S. National Science Foundation
New York State Atomic & Space Development Authority
New York State Science & Technology Foundation
U.S. Air Force Office of Scientific Research
Advanced Research Projects Agency

Such support does not imply endorsement of the content by any of the above parties.

April 1976

A B S T R A C T

A scheme for population inversion in the soft x-ray ($\geq 100\text{Å}$) region where the upper laser level is photoexcited by resonant line radiation from an identical or different ion species is proposed. Ion pairs that may be used in this scheme are presented. Applying the results obtained for a general case to the Mg XI1 ions pumped by CV1 ions, it is shown that gains in excess of 100cm^{-1} are possible for the 4→3 transition at $\sim 130\text{Å}$ in typical laser produced plasmas.

Numerous proposals for producing a population inversion on soft x-ray transitions have recently been published.[1] In this paper we will consider resonant photoexcitation for this purpose. Two approaches are discussed. In one, the upper laser level is preferentially populated by enhanced photoexcitation to this level using resonant radiation from a specified source ion. In the other, the photoexcitation to the lower laser level and hence its population is suppressed by absorbing the radiation resonant with it, but leaving the photoexcitation to the upper laser level relatively undisturbed. The present work differs from recently published photoexcitation schemes[2] in that the schemes discussed here satisfy the resonance condition exactly or well within the ion line widths present under normal laser plasma conditions.[3] Also the scheme described here is scalable along the isoelectronic sequence without seriously deviating from resonance.

The proposed photoexcitation arrangements are shown schematically in Figure 1. Figure 1a shows a two step process involving ion population transfer from ground state (n=1, where n is the principal quantum number) to the first excited state (n=2) and then to the upper laser level (n=4) by photoexcitation. The photoexcitation is by radiation from a source ion at λ_1, which is nearly resonant with λ_p. In Figure 1b the radiation at λ_1 from source ions is filtered by selectively absorbing ions or atoms with absorbing wavelength λ_F nearly resonant with λ_1 and the radiation at λ_2 is used to photoexcite identical ions placed to receive the filtered radiation only.

For observable gains with the above inversion schemes, we need (1) large population in the photo absorbing level (2) the simultaneous existence of source and lasing ions (as well as filtering ions in case (b)) in the plasma environment (3) large photo-absorption cross-sections

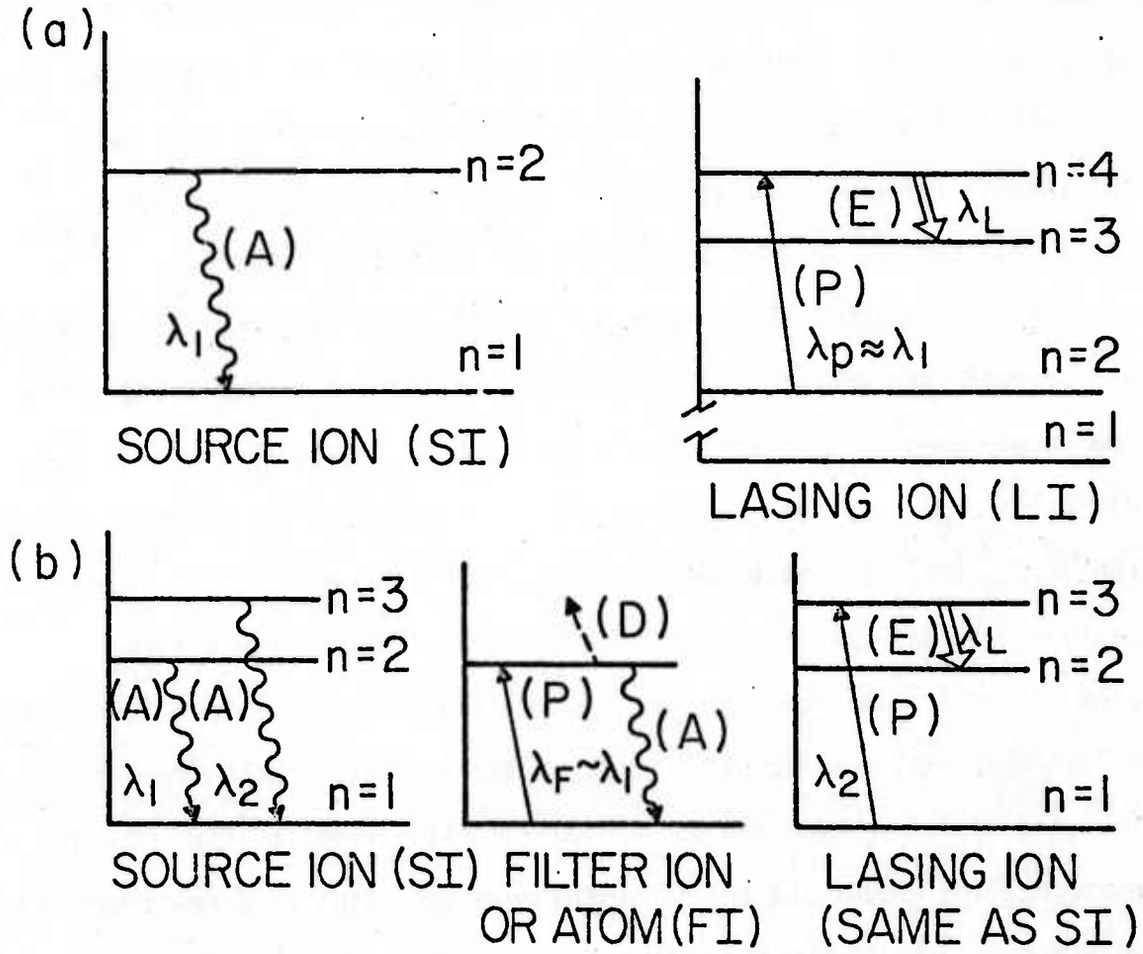

Fig. 1 Schematic diagram of various photoexcitation schemes. (A), (P), & (E) are the relevant radiative decay, photo-excitation, and stimulated emission processes. The process (D) indicates a decay process other than radiative decay back to ground state. We want this process to be orders of magnitude greater than radiative decay back to ground state. Once such process is auto ionization.

and (4) high degree of resonance between the source radiation and the photo-absorbing transition. Point (4) is probably the most important consideration since the photoexcitation rate and source utilization depend very strongly on the degree of resonance. The scheme (b) naturally satisfies the above requirements to a large extent and in scheme (a) it will be shown that by using the steep temperature profiles and large collisional radiative excitations[3] in the laser produced plasmas, points (1) and (2) in addition to (3) and (4) may be satisfied.

In Table 1 some of the hydrogen-like, helium-like, and lithium-like ions paired according to the schemes (a) and (b) are listed along with the wavelengths,[4] the resonance mismatches ΔE_M (ev), the doppler widths[6] ΔE_D (ev) at an ion temperature of 400eV and the stark broadening[6] ΔE_S (ev) at an ion density of 10^{20} cm^{-3} for the selected transitions. In (a) Lyα in hydrogen-like ions and the resonance line W(2p'P -1s'S) in helium-like ions are considered as the source radiations. H_β and λ(2p -4d) are the wavelengths of the photo-absorbing transitions from n=2 to n=4 in hydrogen and helium-like ions respectively. We see that the line widths and the fine structure splitting of a few tenths of an electron volt in the hydrogenic ions more than cover the resonance mismatch in most cases. Also we notice that scheme (a) offers the largest number of energy coincidences over the range of ions surveyed. The best coincidences occur for hydrogenic ion pairs where the atomic number of the lasing ion is twice that of the source ion.

Because of the scalability of scheme (a), we have used a set of coupled equations to estimate the steady state pump radiation density required to invert hydrogenic ions in this scheme. These equations, valid for a lasing ion with atomic number Z, are

(a)

SI		H-LIKE 'LI'					He-LIKE 'LI'			
Z	$Ly\alpha$ W(2p-1s)	Z	H_β	λ_L	ΔE_M	ΔE	Z	λ(2p-4d)	λ_L	ΔE_M
4	$Ly\alpha$=75.928 W=100.2552	8 7	75.890 99.13	~293 382	.07 1.1	$\Delta E_D \approx .07$ $\Delta E_S \sim .8$	9 8	76.512 100.253	~294 385	-0.8 2×10^{-3}
5	48.587 60.3144	10 9	48.55 59.95	188 231	.16 1.0	0.1 0.8	11 10	60.447	234	- .4
6	33.736 40.2680	12 11	33.70 40.11	130 155	.3 1.0	0.13 0.8	13 12	33.94 40.42	130 156	-1.8 -1.0
7	24.781 28.787	14 13	24.74 28.70	96 111	.7 1.1	0.16 0.8	15 14	24.96 29.013	96 115	-2.9 -2.7

(b)

LI	λ_I	FI	λ_F	λ_L	ΔE_M
BIV(2p-1s)	60.314	NaIX(4s-2p)	60.375	416	-.17
BV(2-1)	48.587	NaIX(5p-2s)	48.553	262	.14

TABLE 1. Source ions (SI), lasing ions (LI), and filter ions (FI) paired according to schemes represented in Fig. 1. Ly_α, H_β are the wavelengths (Å) of the Lyman alpha and Balmer Beta lines respectively and W is the resonance line of Helium-like ions.

$$n_1 \left[C(1,n)+B(1,n)\ P_\nu(1,n)\right]$$

$$= -n_n \left[\eta\left(S(n)+\sum_{m\neq n} C(n,m)+\sum_{m\neq n} B(n,m)\right) P_\nu(n,m)+\sum_{m>n} A(n,m)\right]$$

$$+\eta\sum_{m\neq n} n_m\ C(m,n)+\sum_{m>n} n_m\ A(m,n)+\sum_{m\neq n} B(m,n)\ P_\nu(m,n)$$

$$- n_n\ c(n,5)\ \delta_{4n} \qquad (1)$$

$$n,m = 2, 3, 4$$

where δ is the kronecker delta, n and m are the principal quantum numbers of the excited levels with population densities n_n and n_m; S(n), C(n,m), A(n,m) and B(n,m) are respectively the collisional ionization, excitation (or de-excitation) and Einstein radiative coefficients[5] from the corresponding levels for atomic hydrogen. Here $\eta = n_e/Z^7$, $\theta = T_e/Z^2$ and $P_\nu = p_\nu/Z^6$ are reduced electron density, electron temperature and the radiation density at the transition frequency ν_{nm} respectively. N_e and T_e are the actual electron densities and temperatures and p_ν the actual radiation density at frequency $Z^2\ \nu_{nm}$ for the lasing ion with atomic number Z. This model is similar to the collisional radiative model of Bates[5], except that here photoexcitation and induced transitions are included by assuming the local radiation densities; the contributions by cascading from $n\geq 5$ and recombination contributions are neglected. In this analysis a range of values are given to the reduced parameters θ, η and P_ν to determine the plasma conditions that lead to inversion between n=4 and n=3 levels. Since the source radiation P_ν (2,4) can be varied independently, we need to assume value for P_ν (2,4) in addition to the resonance radiation density P_ν (1,2) of the lasing ion. The other radiation densities are scaled from P_ν (1,2) by corona model.

The results of the analysis are presented in Figure 2. Even though the ground state density of hydrogenic ions depends on θ, we find that the effect of temperature on the excited state density ratios n_2/n_1 etc. is minimal in the range $2.8\times10^8\ ^oK < \theta < 5.2\times10^4\ ^oK$. Hence only results at $\theta=4.2\times10^4$ (^oK)are presented. In Figure 2a the dependence of maximum η for inversion between n=4 and n=3 levels is given as a function of the source radiation density P_ν (2,4), with P_ν (1,2) as the parameter. It can also be viewed the variation of the threshold P_ν (2,4) (at which $g_3n_4 = g_4n_3$) for different η. We note that threshold radiation density values increase rapidly as η and P_ν (1,2) are raised. This is due to the increasingly more effective collisional excitation to n=3 level from n=1 and n=2 levels. In Figure 2b and 2c, the effect of P_ν (2,4) on the fractional inversion density, $\left[n_4-(g_4/g_3)n_3\right]/n_1$, and the photoexcitation ratio n_4g_3/n_2g_4 is shown with η as the parameter. In Figure 2b the comparison of the fractional inversion density at P_ν(1,2) values of 3×10^{-12} and 3×10^{-13} erg/cm^{3}Hz shows that a considerable fraction of the lasing ions can be excited to n=4 level by the two step process of collisional radiative excitation. Figure 2c shows the effectiveness of the photoexcitation in transferring population from n=2 to n=4 level at various radiation densities.

In addition, the following conclusions can be drawn from Figure 2. (i) Photoexcitation effects are quite pronounced at a low electron density as indicated by the lower threshold radiation densities, higher fractional inversion density and higher photoexcitation ratio (ii) Threshold (where photoexcitation and collisional processes become comparable) and saturation (because of the statistical equilibration of n=2 and n=4 level populations) effects are noticed in both fractional inversion density and photoexcitation ratio. But we should point out that saturation

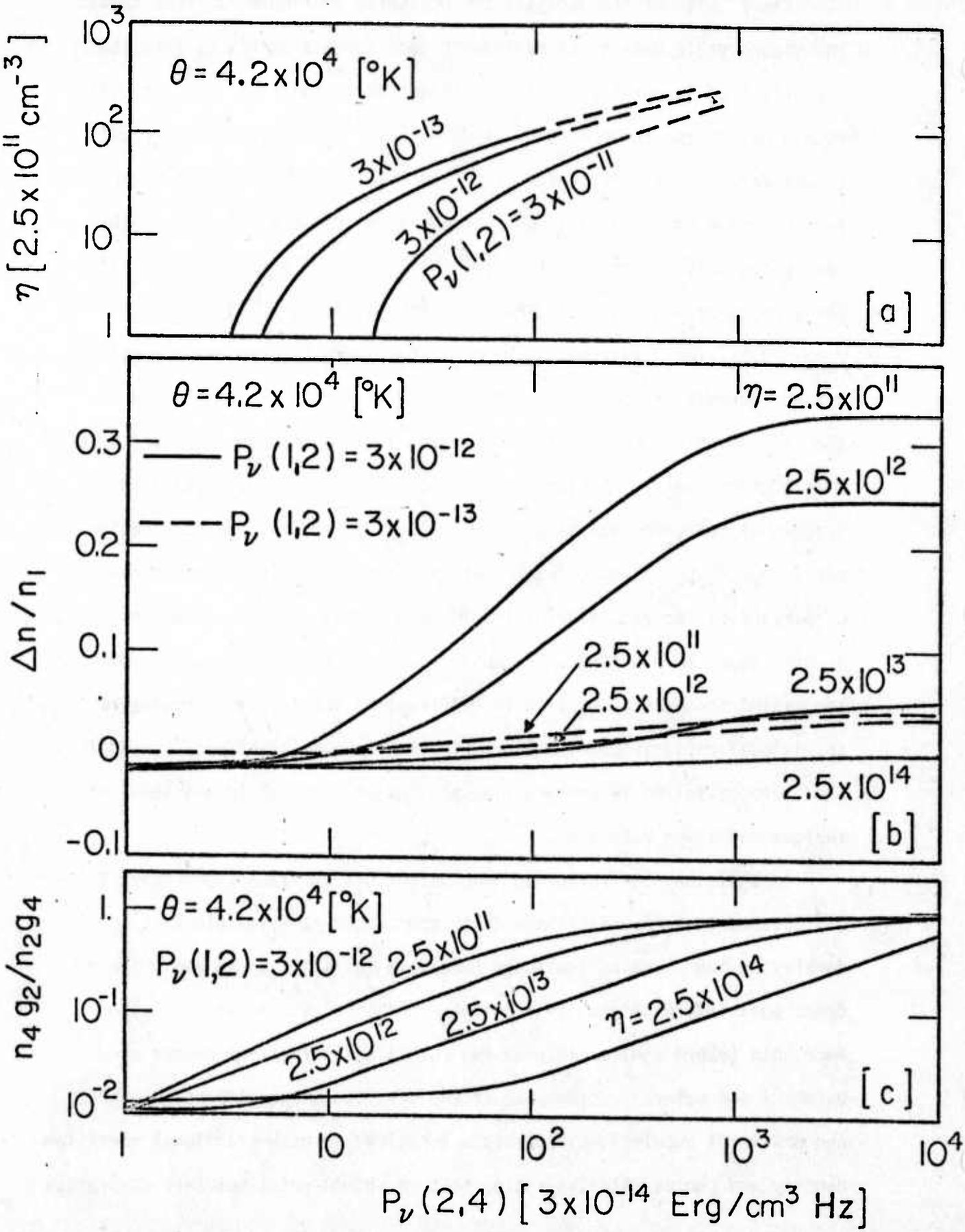

Fig. 2 Results of excited state model. (a) The maximum reduced electron density $\eta(cm^{-3})_3$allowed for inversion to occur vs. the source radiation density $P_\nu(2,4)$ (erg/cm^{3}Hz) with the resonance line radiation density, P_ν (1,2) (erg/cm^{3}Hz) as the parameter. (b) The fractional inversion density ($\Delta n/n_1$), and (c) The

effects are reached at high intensities (iii) For a given P_ν (2,4) and n, radiation density P_ν (1,2) and hence P_ν (1,3) has a value above which inversion is not possible (Figure 2a). Hence a minimum source to lasing ion density ratio is needed for inversion to occur.

As an illustration, the results of Figure 2 are applied to lasing ion with atomic number Z=12 (Mg) and the following gains (α) are estimated at $\lambda_{34} \simeq 130\text{Å}$ for electron and radiation densities indicated.

$n_e(cm^{-3})$	P_ν (2,4), P_ν (1,2) (erg/cm^3Hz)	Δn (4,3) (cm^{-3})	$\alpha_{4,3}(cm^{-1})$
10^{19}	10^{-5}	10^{17}	~ 90
10^{21}	10^{-5}	2.5×10^{18}	~200

Here the laser transition at λ_{34} is assumed to be stark broadened[6] and the ground state ion population n_1 to be $5 \times 10^{-2}\ n_e$. The radiation density of 10^{-5} erg/cm^{3}Hz corresponds to an x-ray pulse energy of 3×10^{-2}J in 10^{-10} sec from a plasma emission area of 10^{-4} cm^2, the emission bandwidth being 10^{14}Hz.

We notice from the above calculations that large amplifications are possible for ions near Z=10 at electron densities, temperatures, and x-ray photon densities achievable with the existing laser systems.[3,7] We feel that all the schemes presented above are experimentally amenable. For example a target configuration in which a homogeneous mixture of source and lasing ion elements is illuminated by 1.06μ laser light can be suggested for the scheme (a). In this case the low Z source element can emit intense line radiation from the dense cooler regions of the plasma to pump lasing ions in the adjacent hotter regions. It is reasonable to assume that because of the near resonance of the source and absorbing transitions and the geometry suggested above, most of the source radiation

participates in photoexcitation. Finally, unlike the electron pumped schemes the photoexcitation schemes proposed here are easy to verify with respect to inversion. For example, observation of anomalous intensities in all transitions from upper photoexcited level in the presence of source radiation (see Figure 2c) is a suitable diagnostic.

ACKNOWLEDGEMENT

This work has been supported partially by ARPA Grant No. N00014-67-A-0398-0017 and DAHC04-71-C-0046 and partially by NSF Grant No. GK-39040X1. The author wishes to thank Dr. M. Lubin and other members of the x-ray group in the Laboratory for Laser Energetics for their helpful discussions.

REFERENCES

1. M. A. Duguay, Laser Focus, Nov. 1973, p. 41; G. Chapline and L. Wood, Physics Today 28, 40 (1975); J. M. Forsyth, T. C. Bristow, B. Yaakobi, and A. Hauer in "Recent Advances in Laser Physics", ed. by M. Sargent, M. O. Scully, and W. E. Lamb, Jr., Addison Wesley (1976)
2. A. V. Vinogradov, I. I. Sobelmann and E. A. Yukov, Sov. J. Quant. Electron, 5, 59 (1975); B. A. Norton and N. J. Peacock, J. Physic. B Atom Model 6, 989 (1975)
3. M. Galanti, N. J. Peacock, B. A. Norton and J. Puric, Fifth Conference on Plasma Physics and Controlled Nuclear Fusion Research, Tokyo, Japan (1974)
4. Atomic and Ionic Emission Lines Below 2000 A, NRL Report 7599
5. D. R. Bates, A. E. Kingston and R. W. P. McWhirter, Proc. Roy. Soc A257, 297 (1962)
6. R. C. Elton, NRL Report 2906 (1974)
7. M. Lubin, E. Goldman, J. Soures, L. Goldman, W. Friedman, S. Letzring, J. Albritton, P. Koch, & B. Yaakobi, Proceedings 5th IAEA Plasma-Fusion Conference on "Plasma Physics and Controlled Nuclear Fusion Research" (Tokyo, Japan (1974)), Vol. II, pgs. 459-477.

DIRECT OBSERVATION OF POPULATION INVERSION BETWEEN Al^{+11} LEVELS IN A LASER-PRODUCED PLASMA

Report No. 63

V.A. Bhagavatula and B. Yaakobi

ACKNOWLEDGEMENT

The research reported on herein was supported by the following principal sponsors:

Exxon Research & Engineering Company
General Electric Company
Northeast Utilities Service Company
University of Rochester

Others contributing to the efforts of the work in the Laboratory for Laser Energetics include:

Empire State Electric Energy Research Company
U.S. National Science Foundation
New York State Energy Research & Development Administration
New York State Science & Technology Foundation
U.S. Air Force Office of Scientific Research
Advanced Research Projects Agency

Such support does not imply endorsement of the content by any of the above parties.

OCTOBER 1977

ABSTRACT

Measured x-ray intensities of the resonance line series of Al^{+11} in a laser-produced plasma shows population inversion between the n=4,5 levels and the n=3 level at a plasma density $N_e \sim 10^{20} cm^{-3}$. The cooling of the expanding plasma leading to inversion is enhanced by a special target configuration. The gain coefficient in the 4→3 transition at 129.7 Å is estimated to be $\sim 10\ cm^{-1}$, using both measured line intensities and numerical simulation.

Population inversion in an expanding laser-produced carbon plasma has been reported in two previous experiments.[1,2] Here we report on the observation of population inversion of the levels n=3 and 4 (also of n=3 and 5) of Al^{+11} by measuring the x-ray lines from these levels to the ground state. Even though the basic mechanism producing the inversion (i.e., recombination in an expanding plasma) is the same, there are several important differences between this and previous experiments:

(1) Here the observed line ($1s^2$-1s4p) starting on the upper level is actually stronger than the line ($1s^2$-1s3p) starting on the lower level of the inverted pair, beyond a certain distance from the target. This means that the deduced population inversion is not subject to doubts because of the imprecise knowledge of film calibration. Similar evidence was reported recently by Dixon and Elton[3] in a different inversion scheme: resonant charge exchange.

(2) Our spectra represent a single experiment per exposure.

(3) By employing a laser of power one to two orders of magnitude higher, we were able to achieve inversion in a higher-Z target (Al as compared with C). Consequently, we observe an inversion at a higher density, $N_e \sim 10^{20}$ cm^{-3}, as compared with $\sim 10^{17}$ cm^{-3} in reference 1 and $\sim 10^{19}$ cm^{-3} in reference 2. Higher densities lead, of course, to a higher gain.

(4) We employ a full-fledged hydrodynamic numerical code rather than a similarity model as in references 2 and 4, and we come to different conclusions: cylindrical expansion is not really advantageous over planar expansion. The expanding plasma in both cases goes through a

similar succession of parameter values (temperature, density, population); only in plane expansion this is extended over longer time and distance spans.

(5) The most important feature of the present experiment is the employment of a stepped target designed to cool the plasma at a certain distance from the initial surface. The idea here is that unlike expansion, cooling due to an additional plate is not accompanied by a drop in density and with it in gain.

Figure 1 shows the experimental configuration: a glass:Nd laser of energy typically 10J in 200psec is focused onto a stepped target: an aluminum slab and a magnesium plate in front of it for cooling the expanding Al plasma. An x-ray crystal spectrograph equipped with a slit measures Al and Mg lines as a function of the distance perpendicular to the target.

Figure 2 shows the aluminum spectra before calibration at two distances from the aluminum surface. The line $1s^2$-1s4p was found to be consistently stronger than the $1s^2$-1s3p line for all distances $\gtrsim$300μm, showing unequivocally an inversion between the n=4 and 3 levels. For larger distances ($\gtrsim$500μm) even the line $1s^2$-1s5p becomes more intense than the two preceeding ones. For smaller distances but larger than 150μm we derive population inversion of the n=3,4 levels even though the line intensities themselves decrease along the series. Flat (non stepped) targets of Al or Mg do not show such intensity inversion (even though some population inversion was deduced). This behavior is consistent with recombination in a cooling plasma which

will show population inversion if $N_e \lesssim 10^{14}Z^7$ (so that excitation collisions are unimportant[5]), the temperature is sufficiently low and the density ratio $Q = n(Al^{+12})/n(Al^{+11})$ is sufficiently high. This means the relative "freezing" of the Al^{+12} ions density which provides the pumping source for the inversion.

We compare the experimental results with the one-dimensional two-temperature hydrodynamic code SUPER[6] which includes an atomic physics group of subroutines similar to what is described in reference 4: rate equations for the evolution of Al ions charge states and excited level populations, and the escape factor approximation for line radiation transport.

Figure 3 shows that the plasma expands in a narrow axial channel (this was also found by Feldman et al.[7]): line widths obtained by the non-focusing spectrograph are determined by the source width. Figure 3 indicates a plasma width $\lesssim$200μm over a large distance (>500μm) from the target. A numerical simulation assuming a planar expansion is therefore justified. Also, the lines intensity decay with distance is found to be consistent with planar, but not hemispherical expansion.

Figure 4 compares measured and computed profiles of T_e. The measured intensity ratio of the Al^{+12} to Al^{+11} resonance lines drops faster with distance when the Mg plate is added. This is evidence of additional cooling due to the plate. The temperature was derived from such curves and the intensity ratios of the inverted lines, using the tables in reference 5. For the recombination regime pertinent to our case we need two intensity ratios for the two coupled parameters T_e and Q. As seen,

the code reproduces well the measured T_e of a flat target; however, the addition of the Mg plate causes T_e to fall faster. To model this cooling in the code we assumed a lateral temperature gradient scale of 200μ, conducting heat into a sink of $N_e=10^{21}$ cm^{-3} at a location corresponding to the Mg plate. This is an approximate model designed only to show qualitatively the effect of additional cooling.

Figure 5 shows the ratio of reduced populations (i.e., after division by the statistical weights) for the n=3,4 shells derived from the measured line intensities. N_e is derived from the ratio $P=I_R/I_C$ (see Figure 3). Note that only if exchange is included in the excitation cross-section[8] can P be <1, as observed. We see that inversion exists in a region where $N_e \sim 10^{20}$ cm^{-3}.

Finally, we show in Figure 6 a sample calculation of population density evolution, with and without additional cooling. There is no inversion at 130μm because the streaming plasma arrives there, first, with too high a temperature, then with too low a Q. Cooling increases the inversion density considerably, which agrees with the observed effect of the Mg plate. Figure 6 also shows that spatial resolution at these distances is partially equivalent to temporal resolution. Using either the calibrated line intensities or the curves "with cooling" in Figure 6, we estimate the gain coefficient for the 4^3F-3^3D manifold[9] at 129.7 Å to be ~10 cm^{-1} which for the measured plasma width ~200μm yields a gain of exp (0.2).

In conclusion, we find that plasma expansion far from a flat target is one-dimensional and shows population inversion via recombination. The addition of a plate in front of the target is found to both cool

the plasma and increase the inversion to give an average gain coefficient of ~10 cm^{-1}. A one-dimensional simulation code was able to reproduce quite well the experimental results (Figures 4 and 5). The present experimental arrangement brings us much closer to being able to observe gain in soft x-ray transitions.

The authors gratefully acknowledge the continuous guidance and intensive discussions with Professors J. Forsyth and M. L. Lubin. Portions of this work were supported by the AIR FORCE OFFICE of SCIENTIFIC RESEARCH under grant (AFOSR-77-3) 189 and ARPA under grant DAHC04-71-C-0046.

References

(1) F. E. Irons and N. J. Peacock, J. Phys. B. 7, 1109 (1974).

(2) R. J. Dewhurst et al., Phys. Rev. Lett. 37, 1265 (1976).

(3) R. H. Dixon and R. C. Elton, Phys. Rev. Lett. 38, 1072 (1977).

(4) G. J. Pert, J. Phys. B. 9, 3301 (1976).

(5) R. P. McWhirter and A. G. Hearn, Proc. Phys. Soc. London 82, 641 (1963).

(6) E. G. Goldman, Plasma Physics 15, 289 (1973), and University of Rochester, LLE Report #16, (1974) (Unpublished)

(7) U. Feldman et al., J. App. Phys. 47, 1341 (1976).

(8) A. V. Vinogradov et al., Sov. J. Quant. Electron. 5, 630 (1975); a revised version in Preprint 121, Lebedev Institute (1977).

(9) R. D. Cowan, Los Alamos Scientific Lab., private communication.

Figure Captions

Fig. 1 The experimental configuration.

Fig. 2 Aluminum spectra from a stepped target (spatial resolution 50μm). The lower spectrum shows inversion of the (1s3p, 1s4p) pair.

Fig. 3 The resonance (I_R) and inter-combination (I_{IC}) lines of Al^{+11} (spatial resolution 38μm). S:dielectronic satellite.

Fig. 4 Computed and measured T_e as a function of distance from the Al surface. Lower curves: intensity ratios of the hydrogen-like to helium-like Al ions resonance lines.

Fig. 5 Axial distribution of: (a) reduced population ratio and (b) computed and measured N_e.

Fig. 6 Code calculation of reduced population densities. Distances are from initial Al surface.

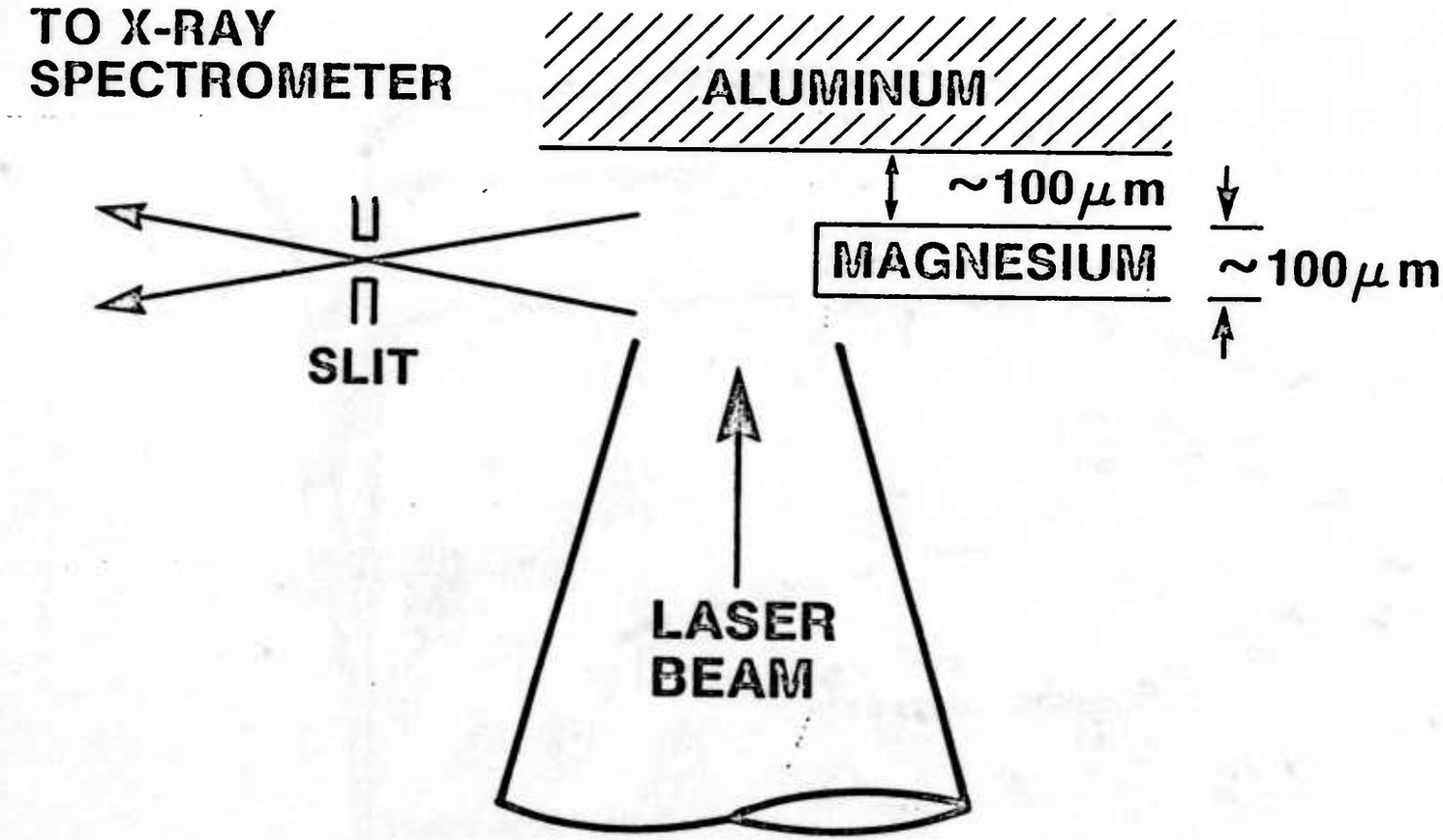
TO X-RAY
SPECTROMETER
ALUMINUM
~100μm
MAGNESIUM
~100μm
SLIT
LASER
BEAM

Figure 1

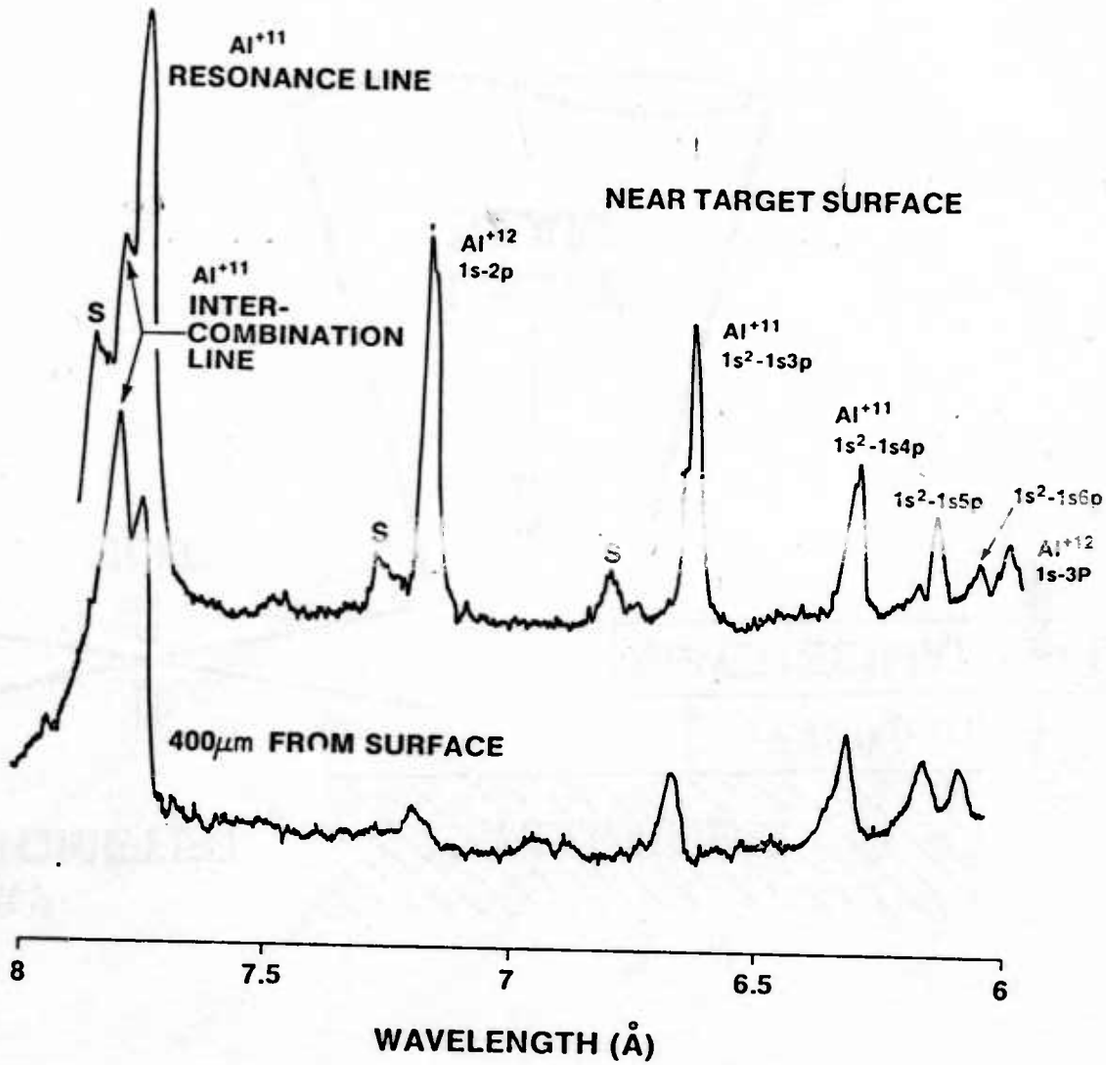
Al+11
RESONANCE LINE
NEAR TARGET SURFACE
Al+12
1s-2p
Al+11
INTER-
COMBINATION
LINE
S
Al+11
1s2-1s3p
Al+11
1s2-1s4p
1s2-1s5p
1s2-1s6p
Al+12
1s-3P
S
S
400μm FROM SURFACE
8
7.5
7
6.5
6
WAVELENGTH (Å)

Figure 2

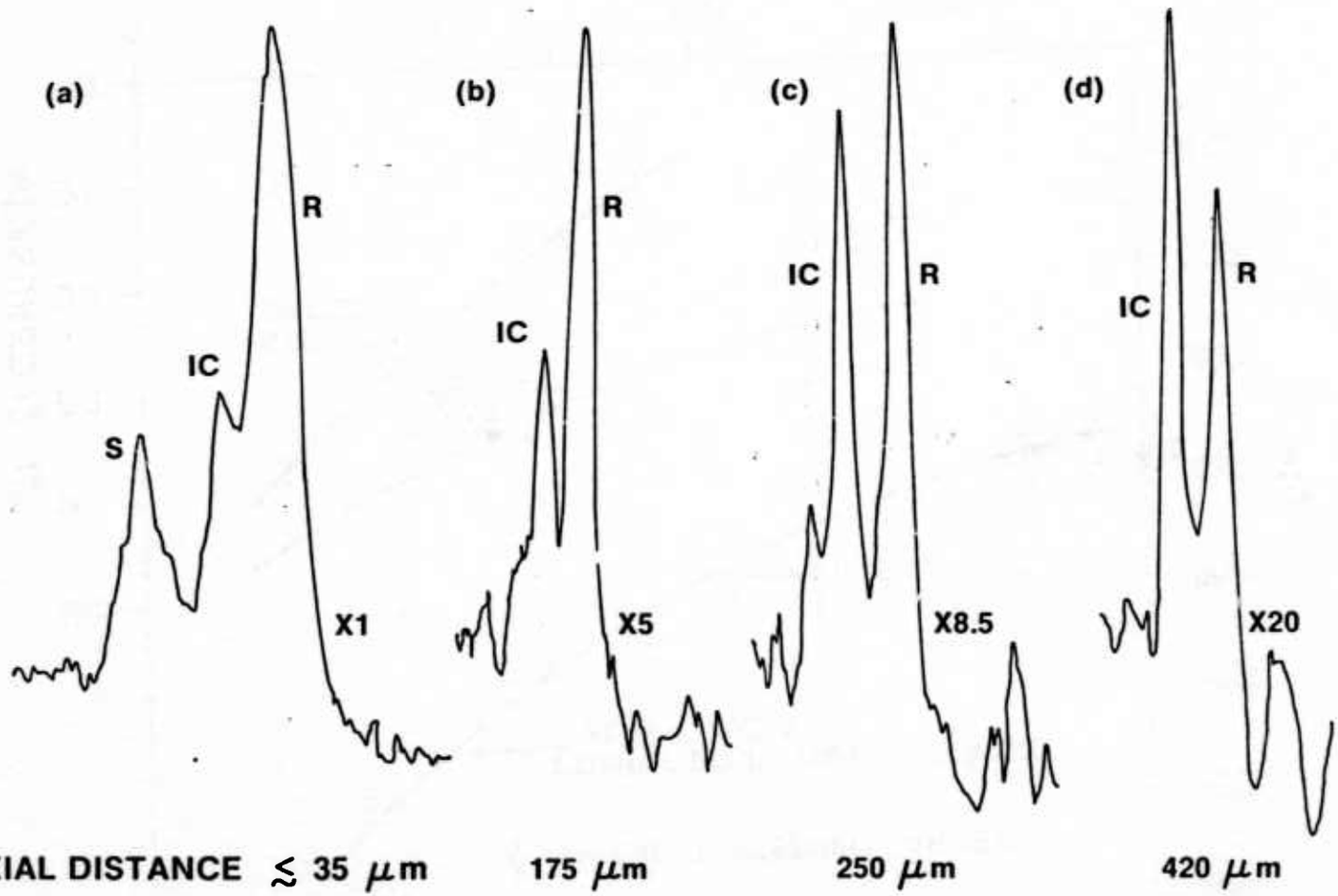
(a)
S
IC
R
X1
(b)
IC
R
X5
(c)
IC
R
X8.5
(d)
IC
R
X20
AXIAL DISTANCE ≲ 35 μm
175 μm
250 μm
420 μm

Figure 3

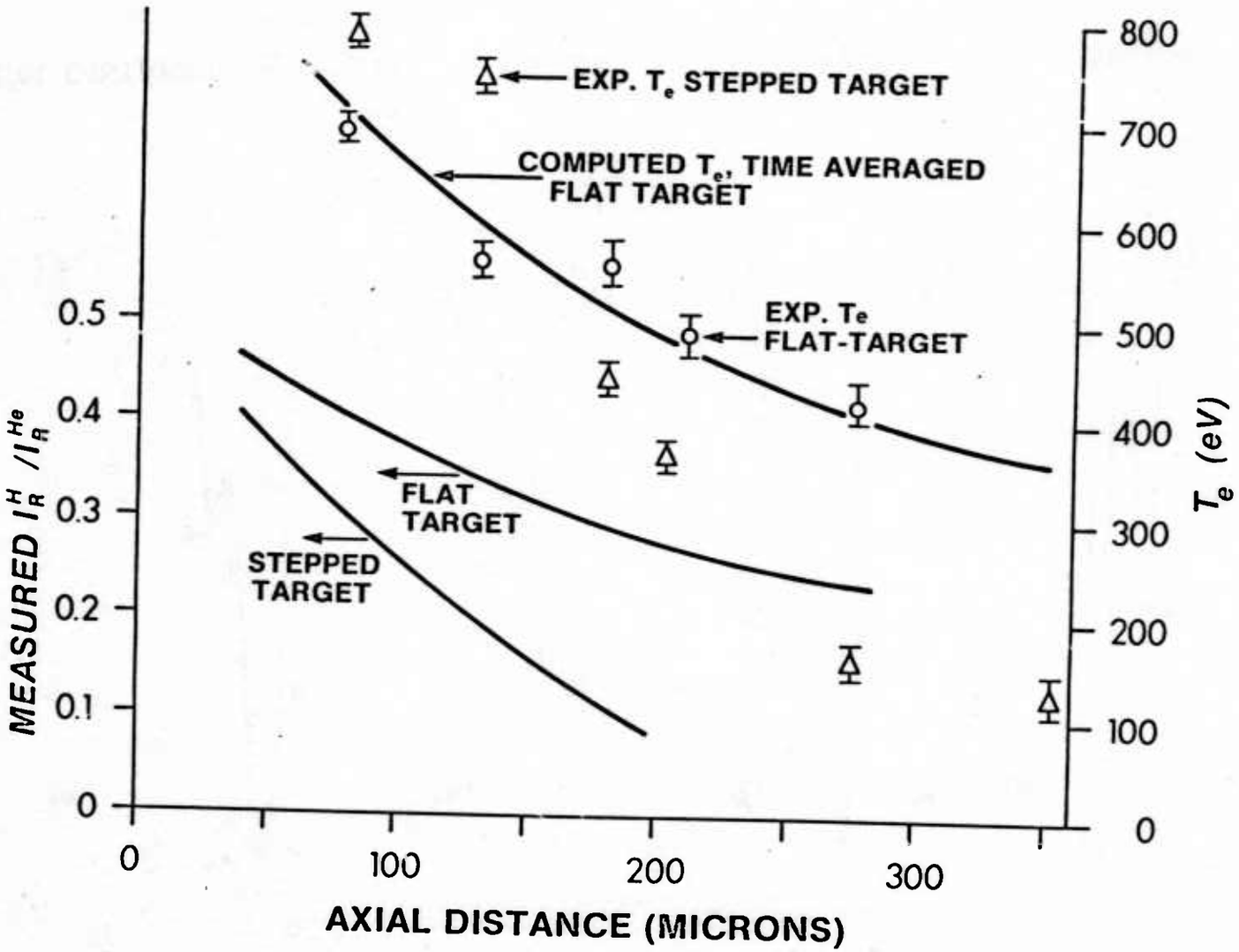
EXP. T_e STEPPED TARGET
COMPUTED T_e, TIME AVERAGED FLAT TARGET
EXP. Te FLAT-TARGET
FLAT TARGET
STEPPED TARGET
MEASURED I_R^H / I_R^{He}
T_e (eV)
AXIAL DISTANCE (MICRONS)
0
0.1
0.2
0.3
0.4
0.5
100
200
300
400
500
600
700
800

Figure 4

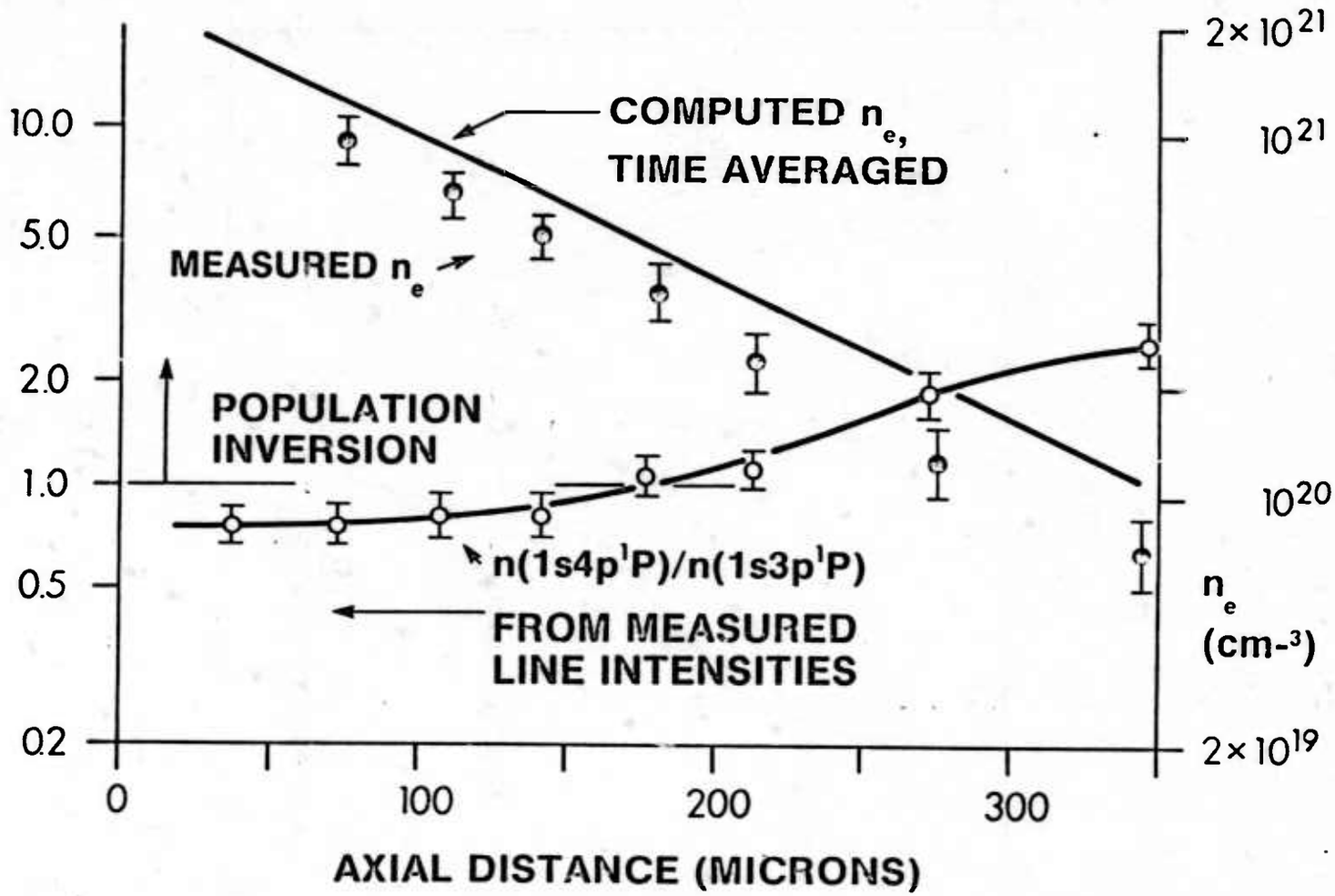
COMPUTED n_e, TIME AVERAGED
MEASURED n_e
POPULATION INVERSION
$n(1s4p^1P)/n(1s3p^1P)$
FROM MEASURED LINE INTENSITIES
10.0
5.0
2.0
1.0
0.5
0.2
0
100
200
300
AXIAL DISTANCE (MICRONS)
2×10^{21}
10^{21}
10^{20}
2×10^{19}
n_e (cm-3)

Figure 6

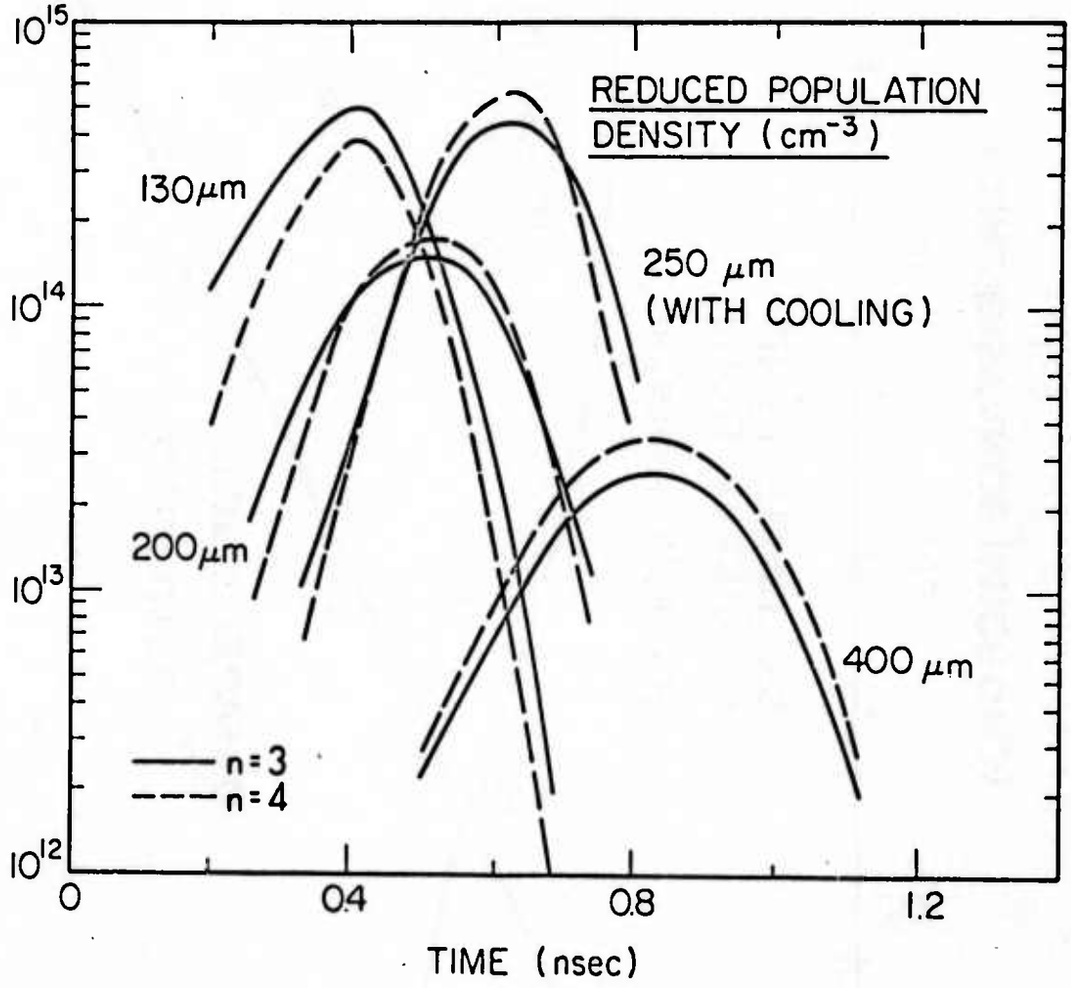
REDUCED POPULATION
DENSITY (cm^{-3})
130μm
250 μm
(WITH COOLING)
200μm
400 μm
n=3
n=4
10^{15}
10^{14}
10^{13}
10^{12}
0
0.4
0.8
1.2
TIME (nsec)

Figure 7

SOFT X-RAY AMPLIFICATION IN A LASER-PRODUCED PLASMA: A REVIEW AND PROGNOSIS*

by

J.M. Forsyth, T.C. Bristow, B. Yaakobi, and A. Hauer

Laboratory for Laser Energetics

University of Rochester

Rochester, New York 14627

This paper is a summary of a tutorial talk presented to the seventh conference on The Physics of Quantum Electronics, Sante Fe, New Mexico, June 23-July 4, 1975. The paper is submitted for publication in Recent Advances in Laser Physics, edited by M. Sargent, M.O. Scully, and W.E. Lamb, Jr., to be published by Addison Wesley.

* Work supported in part by ARPA Contracts N00014-67-A-0398-0017 and DAHC04-71-C-0046.

I. INTRODUCTION

The reader of volume 3 of this series will have a considerable wealth of information immediately available on the very important subject of the use of high peak power laser pulses to heat plasma media to temperatures favoring thermonuclear fusion of hydrogen isotopes. In plasmas where such temperatures exist the conditions may also exist for the efficient production of soft x-ray radiation. Efforts to utilize radiation so produced to optically pump a soft x-ray laser system are described elsewhere in the present volume. It is the intent of this article to discuss the prospects for observing soft x-ray amplification directly in a laser-produced plasma medium.

We will begin with some general remarks on the suitability of a laser heated plasma to produce an amplifying condition. The several mechanisms which can produce x-ray excited states in a plasma will be listed with particular emphasis given to collisional processes. Examples of proposals for achieving inverted populations which rely primarily on one of each of these mechanisms will then be presented.

The number of ideas for development of a soft x-ray laser in a laser produced plasma seems endless; however, most ideas are based on the assumption of a certain convenient, detailed set of plasma conditions. The existence of these conditions has not been experimentally demonstrated (or refuted) in most instances as of this writing. Accordingly, we will discuss efforts to deduce the detailed information on laser plasma parameters required to choose the most promising of the proposed schemes for experimental test. Finally, we will discuss some considerations in the design of an experiment to observe gain in a laser produced plasma.

There is no doubt that a plasma medium is suitable for producing laser action: electric gas discharge lasers are almost as old as lasers themselves.[1] However, there are some important differences between the plasma conditions in, say, a helium-neon laser and laser-plasma conditions. These differences have made it difficult to extend and extrapolate known electric discharge laser schemes using laser plasmas. Laser produced plasmas are typically of rather small dimensions, often occupying a volume 100μm or less across. Gas discharge lasers may have dimensions of meters or larger in some cases. Interestingly, the total number of excited atoms or ions in the two cases is approximately the same. Therefore, we must look further for the source of difficulty.

Perhaps the single most important difference lies in the vast difference in particle densities present in gas lasers versus the active region of a laser produced plasma. Electric discharge lasers typically operate with electron densities in the range of 10^{11} to $10^{13}cm^{-3}$ while the active regions in laser plasmas may exhibit electron densities of 10^{17} to $10^{21}cm^{-3}$. It is clear that collision processes will be emphasized differently in the two media. A part of the difference in collision effects arises from the vast difference in particle temperature in the two cases.

At short wavelengths high particle densities are necessary for achieving laser action on all but strictly forbidden transitions. There are two important reasons for this. First, since the lifetimes of excited states for allowed x-ray and extreme VUV transitions are shorter than for transitions at optical wavelengths (see Table 1), a higher rate of production of excited states is required. Secondly, since efficient optical cavities have not yet been designed for short wavelength lasers,

rather high inversion densities will be required just to produce evidence of laser action.

It has been predicted for some time that laser plasma electron densities were more than adequate for very rapid x-ray excited state production.[2,3] The difficulty is to find systems in which this excitation does not result in a normal (i.e., thermal) distribution of excited state populations. This last point may be better appreciated if we consider some of the characteristic time scales for collisional processes in a high density plasma. A time scale of interest here is the time required for an ensemble of colliding particles to develop a Maxwellian velocity distribution.

The classical kinetic theory of a plasma allows us to consider a situation in which the electrons and ions in the plasma have slightly non-Maxwellian velocity distributions and are characterized by slightly different kinetic temperatures.[4] In such a case the electrons will relax to a Maxwellian distribution in a time

$$\tau_{ee} = \frac{3.32\times10^{5}(kT_e)^{3/2}}{n_e \ln\Lambda} \qquad (1)$$

where kT_e is the plasma electron temperature in eV, e is the electronic charge, n_e is the electron density in particles per cm^3 and

$$\Lambda = 1.87\times10^{6}\,\frac{(kT_e)^{3/2}}{(\pi n_e e^{6})^{1/2}} \quad .$$

A Maxwellian distribution will be achieved only if inelastic collisions can be neglected. Of course, the key to exciting a laser is to take advantage of certain inelastic collisions with large cross sections. As

a result the electron velocity distribution is never strictly Maxwellian in a collisionally excited laser system. In most such lasers the effect of the inelastic collisions is to quench the high energy spectrum of the distribution while leaving the low energy spectrum intact. In this case the electron velocity distribution will still relax to its approximately Maxwellian form on the time scale indicated in equation 1. We will take this estimate as a guide in analyzing a laser plasma, recognizing that inelastic collisions may play a more important role here than in a gas discharge.

An important consideration arises for laser development when we consider the exchange of energy between the electrons and ions in the plasma. The characteristic time for such exchange (i.e., the time required for the electrons and ions to come to identical temperatures) is

$$\tau_{e\text{-}i} = \frac{M}{m} \frac{1}{z^2} \tau_{e\text{-}e} \qquad (2)$$

where M is the ion mass, m is the electron rest mass, and ze is the ionic charge. In a low density plasma this time can be longer than the characteristic time for the ions to exchange energy with some heat sink such as the walls of a discharge tube. Thus the ion and electron temperatures may be maintained at substantially different values at low densities. This results in high gain on inverted transitions because of relatively low Doppler widths. On the other hand, at high particle densities the principal coupling of the ions is to the plasma electron cloud. At high densities we must be concerned about the time scale for significant ion heating and the potential degradation of gain.

In Table 2 we list some plasma conditions in a few common gas lasers along with typical laser plasma conditions. The time scales given by equations (1) and (2) in these plasmas are listed for comparison. It is clear that we can expect to avoid significant ion heating in laser plasmas only on a subnanosecond time scale. Moreover, if we have produced hot ions we must expect to wait for at least a nanosecond to obtain significant cooling. Further significance to these numbers will develop as we consider specific proposals for producing laser action in a laser produced plasma.

In Table 3 we compare the linewidths of the laser systems listed in Table 2 with calculated Doppler widths on representative soft x-ray transitions which could be excited in a laser plasma. We have chosen an ion temperature of 200eV for the laser plasma ions. Such a temperature may characterize the higher density regions of such a plasma. It is worth noting that the relative Doppler widths in a laser plasma may be no worse than the relative width of the collision-broadened transition in a hgih pressure CO_2 laser.

In addition to Doppler broadening a contribution to the broadening of spectral lines in a high density plasma arises due to collision processes.[5] Since charged particles are involved, each ion is subjected to the electric field produced by neighboring particles (electrons or ions), leading to a Stark broadening of the spectral line. The broadening contribution from ions is usually treated by the so-called quasi-static approximation in which the ratio of average particle speed to average interparticle distance is small compared to the line profile width of interest. Broadening from electrons is usually treated by the impact

approximation in which the above ratio exceeds the profile width. In either case the Stark width may be equal to or greater than the Doppler widths referred to above. Since particle proximities increase with density, Stark broadening is important at high densities.

Perhaps a more important process in degrading inverted populations are non-radiative transitions induced by inelastic electron-ion collisions. If this collision time is short compared to radiative decay times (or other level pumping times), then level populations will be sustained at thermal equilibrium values. An estimate of the inelastic collision time is given for allowed transitions as[5]

$$\tau_{inelastic} = \frac{10^6 Z^3}{n_e} \qquad (3)$$

where the plasma temperature is assumed to be appropriate for exciting the lines of interest. For the gas lasers listed in Table 1, these times are longer than the relevant radiative lifetimes. For the laser plasmas listed these times are approximately equal to resonance level lifetimes. The choice of plasma density and ion charge state is clearly crucial to the success of any laser plasma inversion scheme.

Having emphasized the important differences between laser plasmas and conventional electric discharge lasers it is worth remembering that none of these differences precludes the achievement of a population inversion in a laser plasma. It does point up the fact that if we are to realize a practical level of gain that we need to be very successful in taking advantage of a selective mechanism for excitation because of large transition linewidths and the short time required to establish thermal equilibrium in high density media. In the next section we will

review the process of production of a high density plasma by a high power pulse of focussed laser energy and discuss the mechanisms for x-ray excited state production. Proposed schemes for producing inverted populations which rely on each of these mechanisms will be given.

II. X-RAY EXCITED STATE PRODUCTION

It would be desirable to discuss the production of x-ray excited states in a laser plasma from the standpoint of detailed knowledge of the plasma parameters. Unfortunately, at this writing we do not have such knowledge and it appears that years of intensive research are still needed in this area. Much of our present understanding of the subject has been supplied by research efforts in laser induced fusion, extensive summaries of which are included in volume 3. For our present discussion it will suffice to rely on a simple model of laser plasma conditions in order to introduce many of the proposed inversion schemes. It is probably fair to say that a major goal in the ultimate development of an x-ray laser is to learn how real plasma conditions will affect the viability of the various proposed schemes and to use this information to design a successful x-ray laser experiment.

When infrared or optical energy is incident on a solid surface with intensities of 10^{11}-10^{12} W/cm^2 or more, a plasma is formed near the surface. At these field intensities free or weakly bound electrons will be accelerated significantly by the intense optical electric field. For our purposes it does not matter whether these free electrons are present due to impurities or due to various ionization processes (including

multiphoton ionization) excited by the incident laser beam. Under the influence of such intense optical fields the free electrons can acquire sufficient energy to ionize neutral atoms or molecules at or near the solid surfaces over a time span of a few optical cycles. The resulting cascade ionization rapidly increases the free electron density near the surface which, in turn, increases the rate of absorption of laser energy.

The details of the development of the plasma during the very early phases have not been extracted from experiments at this writing. However, it is sufficient for our present discussion to visualize the plasma development along the lines shown in Fig. 1. In Fig. 1a we show a particle density distribution, N(x), representing a solid, plane surface at the point x=0. In Fig. 1b some ionization near the surface has occurred, probably on a subpicosecond time scale. In Fig. 1c a plasma density distribution has developed which may become approximately stable in shape (though not fixed in space) depending on the time scale of laser irradiation. The electrons in this plasma can execute oscillations under the influence of plasma electrostatic forces. The frequency of oscillation is proportional to the square root of the particle density. Where the electron density reaches a level (called the "critical" density) such that the electrons oscillate at the same frequency as the applied optical field, incident laser energy is stored in the medium.

The damping of these oscillations excites many processes including particle heating, fast particle acceleration, back scattered radiation at the laser frequency and various harmonics, and radiation of x-rays. As absorption of laser energy continues the particle temperatures are determined by a balance between the rate of delivery of laser energy,

heat conduction by the plasma into the target and the relative importance of the other processes above.

The balance of energy among the various plasma processes depends on many factors such as laser intensity and target composition. The time scale for laser irradiation is also important. Although short time scale irradiation may not optimize total x-ray production by the plasma, it is most likely to avoid significant ion heating (eq.2) and achieve non-thermal level populations (eq.3). Ignoring some details we may picture the plasma electron temperature and density profiles at some instant during short pulse laser irradiation as shown in Fig. 2.

We have divided Fig. 2 into four regions along the abscissa corresponding to various positions with respect to the laser target surface. It may be convenient to visualize a plane target surface with incident laser energy approaching from the right of Fig. 2. Region I represents the solid target material which is not heated significantly during the laser pulse. The electrons in this region may be free or bound depending on the target material.

In region II we show a steeply decreasing electron density profile and a rapidly increasing electron temperature profile. In this region the electrons and ions form a plasma. Heat conductivity keeps the temperature high through the outer zone of region II. With a neodymium laser (λ=1.06μ) the critical density is approximately $n_e=10^{21}cm^{-3}$ while with a CO_2 laser (λ=10.6μ) the critical density is at $n_e=10^{19}cm^{-3}$. Thus the profiles indicated in figure 1 will look quantitatively different in the two cases.

Region III is a low density, high temperature region which can be called the coronal region. The absorption of laser energy is not high

here but the primary loss mechanism is due to expansion which is not effective on very short time scales. Thus the temperature tends to be rather high in this region.

Region IV is an area of essentially free expansion if the target is located in vacuum. There is a negligible absorption of laser energy and the density is becoming so low that collisions become infrequent between the particles. Thus the thermal velocities possessed by particles near the outer edge of the corona become directed velocities of expansion in region IV. Consequently, the kinetic temperature is reduced in this region.

While it is difficult to ascribe sharply defined boundaries to these regions, we can give approximate dimensions to the important central regions. Typically under high power focussed laser irradiation region II will be from a few microns to a few tens of microns in extent while region III may be up to a millimeter or more in extent. In fact, precise measurements of the actual profiles suggested by Fig. 2 is a challenging area of laser plasma diagnostics research.

Having established an approximate environmental framework for our discussion we can list five important mechanisms for producing x-ray excited states in a laser plasma,

1) electron impact collisions
2) radiative and three-body recombination
3) dielectronic recombination
4) photoexcitation
5) charge exchange.

Proposals involving each of these mechanisms have been given to produce population inversions in a laser plasma. Before considering the specifics of such proposals it may be worth connecting these processes with the various regions given in Fig. 2.

Electron impact processes are important throughout most of regions II and III. Because of the wide variation of temperature and density over the region, such processes may offer the widest range of opportunities for excited state production. However, if laser plasma conditions are fairly represented in Fig. 2, then the most energetic x-ray states will be excited in the high temperature area, region II.

Recombination processes also occur throughout regions II and III. However, high-lying bound levels produced in recombination may be collisionally destroyed before significant radiation can occur. Collisional destruction is suppressed at lower densities so that the formation of radiating, energetic states by recombination tends to be favored in the outer edge of region III. Not all recombination processes are favorable to inverting level populations, however. Radiative recombination, in particular, is favored to energy levels of low principal quantum number thus precluding inverted populations. Three body recombination, on the other hand, is favored to levels of higher principal quantum number which should favor the achievement of an inversion. The conditions under which three body recombination may dominate radiative recombination have been discussed in several places.[6,7] It appears that the outer zones of region III may provide the desired conditions at least over a portion of the time history of the laser heating pulse.

In addition to the above processes, dielectronic recombination is also an important mechanism for excited state production in a laser

plasma. In this process the kinetic energy of an initially free electron appears, in part, as orbital energy on recombination and, in part, as additional orbital energy to an already bound electron in the plasma ion. The resulting ion is said to be doubly excited. There are several modes of decay for doubly excited levels, some of which may be strongly radiative. Use of these levels has been proposed in possible population inversion schemes. In a laser plasma, dielectronic capture should be most favored in high density, moderate temperature regions such as the inner zone of region II.

Since laser plasmas are strong x-ray emitters, one would expect photoexcitation to make a significant contribution to excited state production. In particular, radiation trapping is thought to be important in accounting for details in the observed line spectrum from laser plasmas.[8] Because trapping effects increase with ion density they should be most important in region II. However, radiation produced in, say, region II may penetrate to the solid substrate, region I. In such a case direct photoionization of inner shell electrons is possible with the resultant emission of characteristic (e.g., K_α) x-rays. Such photoexcitation is discussed as a mechanism for population inversion in a companion article. However, photoexcitation in the plasma medium has also been proposed to produce inverted populations.

As the hot plasma expands the particle density becomes low and the initial thermal energy is converted into energy of expansion. Neglecting fast particles produced by strong, local electric fields near the target surface, the expanding plasma is electrically neutral. Thus, even though the bulk of the thermal energy may have been possessed by the

electrons, virtually the entire expansion energy is possessed by the massive ions. For a 1 keV (typical) electron temperature in region III, ion expansion energies of 10 keV or more are found in region IV.

Ordinarily region IV represents a transition to hard vacuum in laser plasma experiments. However, it has been proposed that by supplying a weak background gas around the target that the expanding ions in region IV may have sufficient energy to participate in charge exchange collisions with the background gas. The use of charge exchange to selectively populate excited states and obtain population inversion is discussed in a companion article. The use of a laser plasma as the ion source may be a practical alternative to the use of particle beams, especially since large currents of highly stripped ions can be produced from a laser plasma.

We will now review some of the proposals for producing inverted populations on soft x-ray transitions in the ions of a laser heated plasma. While some of these schemes have been subject to experimental investigation, a systematic study of even a limited number of them has not yet been completed. Because of this, even some preliminary results of a negative nature cannot be taken as indicative of the ultimate worth of a particular scheme; nor can some positive results be taken for guidance because of the limited value of the evidence gathered so far. Many of the proposed schemes involve the use of a very high peak power, short pulse laser to heat the plasma medium. Such lasers require expensive and sophisticated facilities found in only a few laboratories. Some of the available facilities are dedicated, at least in part, to other research efforts such as laser fusion, thus further limiting the possible

size of the experimental program. Clearly it will be some time before the schemes discussed here can be thoroughly explored.

Among the most fertile areas for suggested inversion schemes is the use of direct electron collisional excitation. This is true in spite of the fact that few existing lasers rely on this method alone for selective excited state production. (Of these, moreover, some have no x-ray analogue, such as the excitation of vibrational levels of molecules.) However, direct electron impact excitation is the dominant mechanism for excited state production in a laser plasma and will probably be the key first step in any pumping scheme within the plasma. To illustrate the variety of possible approaches with direct excitation we will briefly review two contrasting proposals.

One early proposal suggested that a self-terminating inversion might be achieved in helium-like ions of elements of moderate atomic weight such as oxygen.[9] A two step process was proposed in which one laser pulse would be used to create a plasma with an adequate density of O^{+6} ions and a second pulse would produce rapid heating of the plasma electrons, preferably on a time scale of 10^{-12} seconds (see eq. 3). For $T_e \sim 1$kev preferential excitation of 3p levels should occur relative to the 2s levels for a few picoseconds, inverting the 3p→2s transition. A diagram of this scheme is shown in Fig. 3. Ultimately, the 2s level population will normalize due to radiative relaxation from the 3p and higher levels and due to collisional relaxation from the 2p levels. The peak gain which might be expected will depend on the extent to which direct excitation of the forbidden 1s→2s transitions may be neglected.

Direct excitation of optically forbidden transitions by electron impact is quite probable in some cases and has itself been proposed as

a path to an upper laser level in carbon-like ions.[10] A diagram of the scheme is shown in Fig. 4. In this configuration an inversion is achieved due to a great difference in the decay ratio of the excited states rather than in a significant difference in excitation rates. In particular, the rapid radiative decay rate of the 3s lower level compared to the 3p upper level makes the scheme potentially cw if stable plasma conditions could be attained. This would be a great advantage for experimental diagnosis as well as for many possible applications. However, there are some drawbacks as well, due chiefly to the fact that the laser transition would occur between levels of the same principal quantum number. This means that the system scales slowly to short wavelengths as a function of atomic number and implies a low quantum efficiency. It also means that one cannot take advantage of very high electron densities because of collisional relaxation between the 3p and 3s levels. In the published proposal a maximum electron density of $10^{17}cm^{-3}$ is recommended for the carbon-like O^{+2} ion.[10] If a Nd laser is used to heat the plasma such an electron density may not be realized until region IV in Fig. 2. This would be undesireable because this is a collisionless regime. However, with a CO_2 laser this electron density might appear in region III or even region II and the prospects for success might be higher. Very little attention has been given to matching the wavelength of the laser heating pulse to the desired plasma conditions in published proposals to date.

Proposals for using a recombining plasma to achieve inverted populations have been given by several authors. The common feature of

these proposals is the concept of subjecting a high density plasma to rapid cooling. This permits three-body recombination to predominate over radiative recombination thus favoring the population of higher lying quantum levels. Details of such processes have been calculated for hydrogen-like ions.[6,7,11] In some cases the initial plasma temperature and density are taken a priori without a detailed proposal for achieving the desired initial conditions. For laser plasma experiments this is still acceptable since we do not yet have detailed information of the time histories of temperatures and densities represented schematically in Fig. 2. At the very least the calculations yield certain minimum conditions which must eventually be found in order to achieve an inversion through recombination.

Inversions produced under the assumed conditions are inevitably transient because of the eventual expansion of the plasma to low densities (favoring radiative recombination) and because of radiative and collisional relaxation to lower levels. The time scales for the latter processes are much faster than the plasma expansion time and represent the limiting duration time for a possible inversion. In low Z plasmas the relaxation times are typically picoseconds; inversions have been calculated to the ground state of hydrogenic ions which are even shorter than this.[11] Inversions between excited levels appear to be somewhat longer lived, although of lower density than inversions on ground state transitions.[12] Of course, ground state transitions are more energetic and yield a substantially higher quantum efficiency than excited state transitions.

Evidence of inverted populations in C^{+5} in a recombining, laser produced plasma has been reported.[13] The estimated inversion density was too low ($10^{11} cm^{-3}$) to provide useful gain. If the general character of the distributions shown in Fig. 2 is correct, then the required low plasma temperatures to favor recombination will be found in the outer corona where densities are low. If inversions can be achieved at all, they are likely to be of low density. All such schemes appear to be limited to excited state transitions because thermal conduction times are longer, as a rule, than the relaxation time of inversions on ground state transitions discussed above.

While radiative and three body recombinations lead to the formation of excited states accessible by means of direct collisions, dielectronic recombination leads to the formation of a different class of excited states, i.e., doubly excited states. The use of dielectronic recombination to achieve inverted populations on extreme VUV transitions is one of the earliest proposals for obtaining gain from a laser produced plasma.[14]

Doubly excited levels are states of very high energy for an atom or ion; they usually lie above the ionization energy for one electron. Thus one of the most important relaxation paths for doubly excited ions is the ejection of one excited electron with the simultaneous reduction of the second electron to the ground state. This process is called autoionization, or the Auger effect, and is clearly the inverse process to dielectronic recombination. In addition, one of the two excited electrons may relax with the emission of a photon. The probability of this type of relaxation is usually much lower than the probability of autoionization, but grows strongly with z. Line radiation from doubly excited states is sometimes quite strong from laser produced plasmas

because a high density of doubly excited ions is often achieved.

The spectral lines produced by doubly excited levels in simple ions tend to have energies which form groups slightly below the energies of the characteristic resonance lines of the next higher stage of ionization. Thus lines within such a group are often referred to as "satellites" to the associated resonance lines. However, the simplicity of this satellite structure is lost in complex ions (e.g., moderately stripped, heavy ions).

The direct use of doubly excited levels for population inversion was suggested by Malozzi, et al., on the basis of observations of satellite emissions to the resonance lines in hydrogen-like aluminum ions generated by a very high power Nd^{+3}:glass laser.[15] Experiments of this type are presently being pursued. To obtain a useful inversion one requires large electron densities in such a scheme. The reason is because most of the ions so excited decay by autoionization before a radiative process can begin, so a large formation rate of excited states is required.

To pick candidate transitions, we would seek doubly excited levels with large cross sections for dielectronic capture, i.e., large cross sections for autoionization, as well as having large radiative cross sections. Such levels can be found but a problem often arises. The radiative processes are usually found on transitions either to the lowest lying shell vacancy of the ion or to another excited state with a large cross section for dielectronic capture. The rapid filling of the lower level means in such cases the inversions, if they can be attained, will be very short lived. Further work on this scheme may be

fruitful, however, since we presently have reliable cross section data for only a very limited number of doubly excited levels on a rather limited list of ions.

Whether or not dielectronic recombination leads directly to the formation of an upper laser level, cascade decay from doubly excited states may be an effective laser pumping mechanism. For example, when one of the two excited electrons decays to the lowest available shell vacancy, a singly excited ion remains. The formation rate of this singly excited level may be rather different than would be true for direct collisional excitation. Thus the level population could be made larger by this mechanism than on other levels accessible only by direct excitation.

Jaegle and coworkers have interpreted certain line emissions from a laser-produced, two plasma experiment as caused by inverted populations.[14] The excited state formation is interpreted as occuring by cascade from autoionizing levels.[16] Their gain observation has yet to be confirmed in other laboratories, but this work shows that cascades from autoionizing levels make important contributions to laser plasma emission spectra and thus can be an important level pumping mechanism.

Whether employed directly or indirectly as a pumping mechanism dielectronic recombination is most important at high electron densities and moderate temperatures. These are present in region II of Fig.2. Depending on the atomic weight of the target atoms the highest stages of ionization may not be present in this region due to the electron temperature distribution. However, the highest ion particle density is present in this region and the total line radiation due to all exciting processes

may be highest from this region. The combination of high radiation density and high ion density means that in this region it is important to consider optical pumping as a possible inversion mechanism.

Absorption of line radiation modifies excited state populations. It is not easy to find discrete transitions in different ions to be in close coincidence, and more difficult still to find a pair of such ions which might be found to coexist under a given set of laser plasma conditions. Therefore, in their proposal Peacock and Norton point out that in a high density plasma, radiation trapping may cause resonance line profiles to exhibit a significantly larger half width due to saturation effects near line center.[17] This effect is sometimes referred to as opacity broadening. These larger effective linewidths can reduce the stringent requirements for energetic coincidence between transitions. Radiation trapping effects require careful analysis because some of the trapped radiation may be lost at high electron densities due to collisional destruction of the excited state.

Norton and Peacock propose using radiation from the $2p \rightarrow 1s$ transition in hydrogen-like carbon to pump the n=4 levels from the ground state of the helium-like carbon ion. This may yield an inversion of population on the $4d \rightarrow 2p$ transition at 186.7Å for a minimum laser power density of 3×10^{12} w/cm^2 on a specially constructed target. The use of hydrogen-like and helium-like ions is an advantage since these two ion stages may be made to coexist in laser plasmas for a variety of target materials. Such a scheme also has the advantage of permitting quasi-cw operation since the lower laser level can be a short-lived resonance level of the pumped ion, as in the above example.

All of the possibilities mentioned up to now have drawn on the laser plasma environment because high particle temperatures and densities can be achieved on short time scales using laser irradiation. However, the end product of a laser plasma is a moderately energetic stream of ions which preliminary experimental tests indicate can be distributed over a narrow range of angles relative to the target surface normal when the plasma expands into hard vacuum.[32] By expanding this stream of ions into a neutral gas background instead, charge exchange reactions may be favored which tend to selectively populate excited levels of ion stages formed by the addition of one electron to the original plasma ions (obtained from the background gas).

In the preliminary calculations, Elton, et al., have found promising combinations using hydrogen or helium as the background gas and using hydrogen-like and helium-like ions from light element laser plasmas.[12] Selective pickup into the 3s shell of the ions seems possible for laser plasma expansion energies with inversions produced on 3s→2p transitions in the extreme vacuum ultraviolet.

III. MEASUREMENT OF LASER PLASMA CONDITIONS

The preceeding discussion of excited state production and laser pumping schemes has been highly qualitative. It is hoped that the reader will seek out the more quantitative discussions in the indicated references. However, no matter how reliably we may be able to calculate the rates of excited state production, the usefulness of the calculation ultimately hinges on the accuracy with which we know the plasma conditions. To make reliable gain estimates, we must specify the local particle densities and temperatures, the transition linewidths in the region of interest and, possibly, the ion expansion velocities. It is the purpose of this section to indicate how such information may be obtained in a quantitative manner from a laser plasma experiment.

Two kinds of measurements are available to an experimenter which are non-perturbing. First, there are measurements of the particle spectrum of the freely expanding plasma, including the electron and ion energy[18] distribution, total ion currents,[19] the ion charge state distribution[18] and, possibly, a neutron current and spectrum. Second, there is the measurement of the electromagnetic radiation from the plasma, including optical,[19] ultraviolet, and soft x-ray emission.[20,21]

We will concentrate our discussion on the techniques using extreme VUV and soft x-ray radiation to diagnose the laser plasma. (The other techniques are referred to and described in volume 3.)
This VUV and soft x-ray instrumentation is a natural ingredient in a soft x-ray laser experiment. We thus hope to emphasize the versatility of measurements made in this part of the spectrum.

The assignment of values to plasma parameters from spectral measurements requires an appropriate model of the relevant physical processes in the plasma. One may choose to use an analytic or a numerical approach to this assignment. To make an analytic model tractable, a number of simplifying assumptions must be made. In return for this one can readily predict the trends implied by a systematic variation of experimental conditions. Ultimately, however, a numerical model is needed to build a detailed knowledge of laser plasma conditions. In what follows we will review the use of some simple analytic models for deducing electron temperature and density in a plasma and apply them to a sample experimental spectrum obtained from a laser produced plasma. We will then discuss some of the weaknesses in the analytic models and briefly describe the use of numerical modeling techniques.

We will begin by discussing the spectral signatures of particle temperatures with primary emphasis on electron temperature. We will assume for the present that we are investigating a plasma of uniform temperature and density and reserve the spatial resolution of the information for later discussion. We will also assume that the electron velocity distribution is (locally) approximately Maxwellian. We might hope that this would be true for even moderately short laser heating pulses, say, 50psec. FWHM and electron densities of $10^{20}cm^{-3}$ or so. (From eq. 1 with kT_e=1Kev, $n_e=10^{20}cm^{-3}$ we have $\tau_{ee}=10^{-11}$sec.)

The emission from a laser heated plasma consists of both line and continuum components in the soft x-ray region. The detailed distribution of both components is sensitive to the electron temperature. We will first consider the distribution of the continuum.

Continuum radiation is produced by bremsstrahlung (free-free) and recombination (free-bound) processes. The bremsstrahlung emission coefficient is given by[5]

$$\varepsilon_\nu^{ff} = 1.36\times10^{-41}\left[\frac{\chi_h}{kT_e}\right]^{\frac{1}{2}} \sum_z z^2 n_{iz} n_e g_{ff} \exp(-h\nu/kT_e) \quad \text{ergs/cm}^3\text{sr} \qquad (4)$$

while recombination emission coefficient is given (for hydrogenic ions) by[5]

$$\varepsilon_\nu^{fb} = 1.36\times10^{-41}\left[\frac{\chi_h}{kT_e}\right]^{3/2} n_e \sum_z \sum_n 2\frac{z^4}{n^3} n_{iz} g_{fb} \exp\left[\frac{z^2\chi_h}{n^2 kT_e} - \frac{h\nu}{kT_e}\right]$$

$$\text{ergs/cm}^3\text{ sr} \qquad (5)$$

where χ_h is the ionization potential of hydrogen

ze is the ionic charge

n_{iz} is the population of ions of charge ze

n_e is the electron density

n is the principal quantum level of a recombination transition.

g_{ff}, g_{fb} are Gaunt factors for free-free and free-bound transitions, respectively.

These expressions are valid when $h\nu >> kT_e$, i.e., when looking at the high energy tail of the spectrum. While one process or the other may predominate for various plasma temperatures and ionic compositions, if one examines the radiation at sufficiently high frequency the same spectral dependence will be observed. The observation can be simply accomplished by fitting a broadband detector with a high pass filter, the latter which is conveniently made using thin metallic foils. The transmission of a foil is simply $e^{-k_\nu t}$

where k_ν is spectral mass absorption coefficient and t is the foil thickness. If identical (or suitably normalized) detectors are fitted with foils of different thickness and if the low frequency cutoff of the foil is high enough to make the transmitted spectral distribution proportional to $e^{-h\nu/kT_e}$ then the relative transmission through each foil is given by

$$R = \frac{\int_0^\infty e^{-h\nu/kT_e} e^{-k_\nu t} d\nu}{\int_0^\infty e^{-h\nu/kT_e} d\nu}$$

Elton has computed this ratio for various values of T_e, k_ν, and t and this published data is commonly used, within its limitations, to estimate laser plasma electron temperatures. An example of a series of curves for various temperatures with aluminum foils is shown in Fig. 5.

With moderate-to-high Z plasmas, line emission can easily fall within the transmission window of convenient foils and upset the validity of the above measurement techniques. However, in these cases the line emission itself may be used to estimate the electron temperature if some means for recording a dispersed spectrum is provided. The instrumentation to accomplish this can often be extremely simple as we will see.

Sometimes the mere identification of a prominent series of lines will establish very good limits on the plasma electron temperature. This is due to the fact that the ionization potential does not increase rapidly as electrons are removed from a given shell but does increase greatly as the first electron from a filled shell is removed. If one can record the spectra using a calibrated instrument, then a more refined

estimate of the electron temperature can be obtained. For laser plasma electron temperatures up to 1 Kev and targets of moderate atomic weight, the principal lines from K-shell electrons are usually observed, i.e., the characteristic resonance lines of the helium-like and hydrogen-like ions. If we assume that direct collisional excitation is the chief mechanism for producing this radiation, we could estimate the temperature from the relative intensities of resonance lines of one of the ions. However, we know that recombination processes may be important in exciting higher lying levels of a particular ion, especially at high particle densities. Therefore, when one- and two-electron spectra are present, it is convenient to measure the ratio of intensities of the first resonance line in each series.

The ratio of resonance line intensities from hydrogen-like and helium-like aluminum ions is shown in Fig. 6. Two different assumptions about plasma conditions are accounted for here. In the so-called corona model excited state lifetimes are assumed short compared to collision times, an assumption which should apply at low densities. In the collisional-radiative (CR) model collisional rates may exceed radiative rates for levels with high principal quantum number, an assumption which will apply at high densities. (One consequence of the CR model is the effective lowering of ionization potentials due to contributions from multistep collisional excitation.)

At very high particle densities radiation trapping effects can give misleading estimates of the electron temperature if they are based on line ratio measurements.[23] These effects can be accounted for in the temperature measurement but a knowledge of the particle densities is

required. We will next give a brief review of techniques useful in measuring plasma particle densities.

Several techniques are available to measure plasma particle densities. If a detector is available whose absolute soft x-ray sensitivity is known, and if the electron temperature is known, then a knowledge of the source dimensions allows the ion densities to be deduced from line intensity measurements and the electron density to be deduced from the continuum intensity. Unfortunately, while calibrated detectors are available, an accurate knowledge of the dimensions of the radiating region of a laser plasma is seldom available. Thus, other less direct methods are usually employed.

One possibility is to observe Stark broadening of spectral lines and infer the particle density from the average local electric field produced by an appropriate distribution of particles. However, if ion temperatures are high, Doppler broadening may mask the Stark effect. Instead of observing resonance (e.g., Lyman series) lines one can get more pronounced Stark effects by observing excited state (e.g., Balmer series) transitions at longer wavelengths. The emission intensities on these lines are substantially lower than on resonance lines. Moreover, the theory of Stark broadening in plasmas of moderate-to-high Z ions is still poorly developed.[24] Thus only a few laser plasma density measurements using Stark profiles have been reported.[25]

A density estimate can be made from the Stark effect in some cases without a profile analysis. Noting that the energy levels of high principal quantum number are progressively closer together, then at a given particle density there will be some level at which the Stark

broadening equals the separation to the next higher level. This level, from which discrete line emission is last observable, is said to lye at the Ingliss-Teller limit for the series.[26] The indentification of this level in hydrogen plasmas is one of the oldest methods for measuring plasma particle densities.[27]

To obtain a density estimate in either case, one must calculate the electric microfield distribution seen by a typical ion in the plasma. This calculation is facilitated by the assumption that the plasma particles are essentially stationary during the radiative lifetime of the excited state of interest. However, calculations have been carried out only for the case of singly-charged plasma ions. Ion correlation corrections have only been computed for cases where the Debye length is larger than the interparticle distance. For high-Z ions a satisfactory theory is still under development so that observations of line broadening effects in laser plasma emission must be analyzed with caution.

Another feature of the line emission which can yield density information is the intensity ratio of certain lines. In atoms where a forbidden transition is energetically close to an allowed transition, the intensity of the former is determined by the importance of electron collisional quenching of the level. The intensity ratio of these two lines will depend on the electron density over a certain range.

We may identify the ranges of behavior bounded by t_a and t_f, the lifetimes of the allowed and metastable levels respectively. If the quenching time is smaller than t_a then the intensities of the lines is independent of n_e. If the quenching time is greater than t_f the intensity of both lines is proportional to n_e. However, if the quenching time is between t_a and t_f, then only the intensity of the allowed transition depends on n_e and thus the ratio of the lines is proportional to density.

In laser plasma work a most useful pair of lines in this connection is present in the spectra of helium-like ions. These transitions are the resonance line (sometimes identified by the symbol "w"), $1s2p\ ^1P_1 \rightarrow 1s^2\ ^1S_0$, and the intercombination line (identified as "y"), $1s2P\ ^3P_1 \rightarrow 1s^2\ ^1S_0$. Radiative and collisional processes for these transitions have been carefully studied and an expression for the ratio given as[24]

$$R = \frac{I_w}{I_y} = R_1 + Pn_e$$

where $R_1 = 1.8$ and P is a coefficient which depends on $k\Gamma_e$ and z. The ratio is plotted in Fig. 7 as a function of electron density for two temperatures.

It is clear that the use of the intensity ratios of spectral lines to estimate electron temperatures and densities is a somewhat interactive process, i.e., a knowledge of the electron temperature is needed to estimate density and vice versa. Ambiguities in the analysis can be reduced if more than one pair of lines can be used in each case or if other diagnostics (such as observation of the Ingliss-Teller limit) can be used to cross-check the results.

To illustrate the diagnostics problem we will describe and analyze a laser plasma experiment performed in the Laboratory for Laser Energetics at the University of Rochester. The laser system used to heat the plasma is a multistage, Nd^{+3}:glass laser. It consists of a passively mode-locked Q-switched oscillator, an optical network which selects and transmits a single pulse from the train, and an amplifier system which is decoupled from both internal

feedback and external (e.g., target) reflections. A schematic of the system is given in Fig. 8. With this laser, single pulses with energies up to 20 joules at 100-200 psec. FWHM have been focussed onto solid targets of moderate atomic weights with a 3" diameter f/4 aspheric lens designed and fabricated at the University of Rochester.

Perhaps one of the most difficult parameters to measure in such experiments from the standpoint of the laser system is the diameter of the focal spot of the beam under full power conditions. Aberrations accummulated by the beam on passing through even a moderately large amplifier system such as this one will seriously degrade the focussing properties.[29] By examining the angular widths of the x-ray lines emitted from the target we estimate that the heated region of the plasma is approximately 100μm in diameter. This means that focussed intensities of approximately 10^{15} w/cm^2 are produced by this laser system.

Although such a source of x-rays is hardly infinitesmal, it is sufficiently small to permit the use of a slitless, flat crystal type spectrometer to obtain an adequately dispersed soft x-ray spectrum. A schematic diagram of the geometry of such a spectrometer is shown in Fig. 9. By choosing a suitably oriented crystal from the acid pthalate family (e.g., TAP, RAP, etc.) sufficiently high x-ray reflectivity can be obtained to get a good quality spectrum on a single shot. (This is particularly desireable if the laser pulse energy is not highly reproduceable from shot to shot.) In our experiment the crystal is located approximately 20cm. from the source. At this distance the angular diameter of the source is larger than the angular width of the rocking curve of the crystal and the spectral resolution is source-size limited.

Figure 10 shows a microdensitometer trace of a portion of a spectrum recorded on Kodak no-screen x-ray film when a 7.9 joule pulse with 100psec. FWHM was focussed onto a solid aluminum target. The principal resonance lines from helium-like and hydrogen-like aluminum ions are quite pronounced. Moreover, satellite lines from doubly excited levels in lithium-like and helium-like ions are clearly present, though not fully resolved. Using this spectrum, which is a time- and space-integrated measurement, we will briefly discuss the problem of reducing this data to obtain estimates of plasma electron temperature and density.

Although the recorded spectrum is an integrated measurement, there may be factors at work which tend to localize at least some of the features. Assuming that the spatial distributions illustrated schematically in figure 1 are stationary, then the radiation of lines from a particular ionization stage will be confined to the region characterized by a temperature which just sustains that stage of ionization. The observed lines could thus be localized by a steep temperature gradient, such as shown in region II, Fig. 2. If the temperature is slowly varying, such as shown in region III, Fig. 2, a steep density gradient will tend to weight the strength of the emitted lines toward the high density region, again localizing the emission.

As a first step then it is only necessary to assume that the distributions represented in figure 1 are stationary over the major portion of the laser heating pulse. This assumption must be tested over a variety of conditions, especially including the width of the heating pulse. Such tests are being undertaken in several laboratories

using high speed electrooptic streak cameras to photograph the plasma motions. Elaborate numerical simulations of the plasma evolution are also being used to improve our understanding of these processes. Our own such simulations suggest that under the conditions of the present experiment that the plasma motion is slight over the major portion of radiative activity. We will discuss the data in Fig. 10 from the standpoint of a localized emission region.

To convert the recorded optical density into irradiance, we performed a calibration of the H vs. D curve for no-screen film over the range of soft x-ray wavelengths in Fig. 10. We find that it is important to do this under conditions representing actual usage rather than relying on published data produced, in all likelihood, under different conditions.

Taking the intensity ratio of the helium-like resonance line (w) to the hydrogen-like resonance line (L_α) gives an electron temperature of 530 eV using the CR model as shown in Fig. 6. Recalling that this calculation assumes an optically thin medium, we can check our result using the intensities of the satellite lines labeled j, k in Fig. 10. Gabriel has given a formula for the expected ratio of intensities between the satellites j, k and the resonance line w as a function of temperature.[30] Using this we find that the observed intensity of w is 92% of the value expected at a temperature of 530 eV. Since the plasma should be optically thin to the satellite radiation (the lower level is an excited state) and since the resonance line w should be the most seriously affected by opacity, we conclude that this electron temperature characterizes the radiating region in this experiment.

It is interesting to note that if one attempts to estimate the temperature using the series of intensity ratios of the lines from the helium-like sequence only, progressively higher temperatures are predicted by the corona model. This directly shows that neglecting multistep excitation of high lying levels is not justified.

To estimate the particle density we can compare the ratio of intensities of the helium-like intercombination line (y) to the resonance line (w) in Fig. 10. In this case the estimate will be subject to uncertainties due to the fact that the intercombination line is not well resolved from the resonance line. Using an expanded scale plot of the data in Fig. 10 we can estimate a contribution to the x,y feature from the wings of w assuming a symmetric line shape. The intensity ratio is determined and compared to the plot in Fig. 7. We obtain an electron density estimate of $1.5 \times 10^{20} cm^{-3}$.

It should be pointed out that this estimate is a lower bound since there may be other contributions to the spectral feature label x,y. While the magnetic dipole transition, $1s2p\ ^3P_2 \rightarrow 1s^2\ ^1S_0$, (x) probably makes a negligible contribution to this feature, there are two satellite lines between x, y, and w. Any allowance made for their intensity will, of course, raise the estimated electron density. Because of the various uncertainties, it would be desireable to have slightly better spectral resolution upon which to base this kind of estimate.

From Fig. 10 it is clear that the principal series lines do not extend to arbitrarily high quantum levels and thus the Inglis-Teller relation

$$n_e = \frac{Z^4}{120a_o^3} \; Z^{3/2} n_m^{7.5} \qquad (6)$$

may be applied, where a_o is the Bohr radius and n_m is the principal quantum number of the last discernable line in the series. In both the helium-like series (Al^{+11}) and hydrogen-like series (Al^{+12}) the last discernable line appears to be $n_m=6$. This gives a density of $N=4.8\times10^{21}$ from the helium-like series and $N=6.6\times10^{21}$ from the hydrogen-like series.

The density estimate computed here from observing the disappearance of principal series lines is an upper limit since instrumental effects could mask the presence of higher lying lines. However, when combined with the lower limit supplied by line ratio analysis, it appears that the observed spectrum is radiated most strongly from the region in the vicinity of critical density, $n_e=10^{21}cm^{-3}$. These results are in fairly good agreement with the conditions diagrammed in region II, Fig. 2.

In the above analysis we have chosen to use simple analytic models for the purpose of illustration. Ultimately, it must be recognized that such analysis is incapable of dealing with several aspects of the emission from laser plasmas. For example, an important assumption in these models is the existance of steady state conditions in the plasma. In particular, the electron temperature is assumed to vary in time slowly enough so that the degree and level of ionization of the plasma has the steady state value. For the short laser pulses ($<10^{-10}$ sec FWHM) used in many present experiments this assumption is probably unrealistic.

To improve our knowledge of the plasma conditions, we must combine the use of elaborate numerical simulations of the plasma conditions with time-resolved studies of the soft x-ray emission. Presently x-ray streak cameras are under development in several laboratories and such time resolved emission studies will constitute one of their principal applications.

Although simple spectrometers such as shown in Fig. 9 provide useful information, the recorded spectrum is spatially integrated. We thus cannot obtain a direct comparison with the profiles shown in Fig. 2, for example. We have indicated that the radiating region which gives a spectrum such as shown in Fig. 10 may be localized by various weighting factors. As a result x-ray pinhole cameras and spatially dispersing x-ray spectrometers are being employed in current experiments to image the plasma. The use of such instruments, combined with one and two-dimensional numerical plasma simulations should provide the detailed understanding which will permit the design or optimization of conditions for producing inverted populations on soft x-ray transitions.

IV. DESIGN OF X-RAY LASER EXPERIMENTS

We will now try to give, in general terms, considerations to be taken in designing an experiment to demonstrate the presence of gain in a laser plasma at soft x-ray and extreme VUV wavelengths. Historically it seems that lasers at optical wavelengths were more often discovered than deliberately invented; this may also turn out to be true with x-ray lasers. However, the worker at optical wavelengths has several advantages to discovery not shared by workers at very short wavelengths. First, we cannot ignore the very important advantage of being able to see the emitted radiation, which greatly facilitates the decision making process and allows many possibilites to be explored quickly. Secondly, the use of regenerative feedback permits weakly amplifying systems to oscillate strongly. In this case successful operation can often be demonstrated with a system which is far from optimized.

If one is to have a reasonable chance to verify gain at very short wavelengths one had best not concede too many more points! Therefore, one should probably narrow the search of the promising proposals to either quasi cw schemes or to schemes in which the gain is likely to survive over most or all of the duration of the incident laser heating pulse. This will enable the diagnostic signal, in whatever form, to be dominated by amplifying effects. Since few high power lasers are presently in operation which produce pulses shorter than 20psec., this requirement appears to rule out easy detection of all self-terminating x-ray laser schemes in the near future. Since cw or quasi cw operation requires rapid decay of the lower laser level we are clearly looking for inversions on excited state transitions. This determines some crude limit on the expected laser transition energy, given the presently achievable laser plasma electron temperatures. The experimental results discussed in the previous

section seem to be representative of achievable conditions and imply excited state transition energies of no more than a few hundred electron volts. Thus extreme VUV instrumentation appears to be essential in present short wavelength laser development efforts.

The lack of available regenerative feedback schemes at these wavelengths means that great care will be required to verify the existence of amplification effects. Direct single pass measurements of gain might be attempted using two laser produced plasmas, one serving as a radiation source for the other to amplify. Such experiments have been criticized as lacking straightforward interpretations but in any event are incapable of being as sensitive as a multipass, i.e., regenerative experiment.

The difficulty is further compounded by the fact that overall laser plasma dimensions are small. This means that a high gain coefficient may translate into a small overall amplification factor. While it is practical to irradiate long, filamentary shaped plasmas using cylinder lenses, the transverse dimension of the focal line is still limited by laser beam aberrations in most systems. Thus the focal area of such a system will be large. This reduces the specific focal plane intensity which will limit the plasma temperature and thus the ionization stages achieved. It seems adviseable to recommend maximum plasma lengths between 0.1 and 1.0cm. using presently available lasers.

Given such a length constraint we would feel obliged to seek a minimum gain coefficient between 1.0 and 10.0cm^{-1} to achieve a readily measureable effect. This is very high by conventional laser standards and suggests that special care should be taken to minimize gain degrading

effects such as Doppler broadening of the plasma ions. It seems plan on two step excitation in many experiments. The first step involve the creation of a plasma in the desired stage of ionizat This could be accomplished without the need for a very short pul laser. After an interval sufficient to permit the ion temperatu drop, a second, short pulse may be used to heat the plasma elec If this pulse is short compared to the time scale given in equat then the excitation may take place while keeping the ion tempera thus the Doppler widths low.

If the proposed scheme to be tested appears to work best ov limited range of particle density, it should be kept in mind tha experimenter can control the deposition point of the focussed la pulse by appropriately choosing the laser wavelength. Since hig lasers are available at only a few wavelengths, efficient freque conversion schemes may have to be employed. In a two step excit scheme, the two laser pulses may be chosen at different wavelengt the best effect.

It may be observed that among presently available discharge lasers many of the highest gain systems are of the self-terminat variety. Using a cleverly designed two step excitation scheme, i be possible to overcome our objection to self-terminating syste one proposal, for example, a line focus plasma is created by a t Q-switched laser pulse.[31] Excitation is then accomplished by a second, ultrashort (mode-locked) laser pulse along the axis of plasma. The duration of the excitation pulse may be short compar transit time of the plasma and thus a travelling wave pumping sch effected.

Assuming that gain has been achieved in a laser plasma, we must ask what constitutes convincing evidence of the achievement? The lack of regenerative feedback means that we are denied the observation of a sharply defined threshold effect; this has proved to be a sticky point for experimenters to date. Short of a direct, single pass gain measurement in a plasma we may look for an excitation dependent directionality of the radiation from the particular transition of interest when excited in a filamentary geometry. If the upper laser level were also the upper level of a non-inverted transition (e.g., a resonance transition) then a comparison of the different directional properties of the two transitions would increase certainty. Evidence of line narrowing might be sought if sufficiently high spectral resolution is available. However, all such evidence is ideally acquired on a single shot basis and this often poses a problem in light gathering power.

Less direct but still acceptable evidence of gain might be developed from measurements of level populations. These may be conveniently measured by the strengths of lines emitted from the levels of interest. However, the oscillator strengths and/or transition probabilities must be well known to do this and this is usually true only for resonance lines in the case of highly charged ions. Thus, the conditions on many potentially amplifying transitions may be inaccessible by this method.

In spite of the difficulties associated with the method, we have a preference for the observation of directional effects as an ultimate diagnostic. This stems from the belief that applications for such a light source will ultimately develop from a filamentary geometry of the medium. The observation of a useful effect in this geometry thus hastens the development of these applications.

V. SUMMARY AND CONCLUSION

It was the purpose of this paper to examine the conditions present in a laser produced plasma and to discuss their suitability for providing soft x-ray amplification. A variety of representative proposals were outlined, each of which attempts to exploit different features and regions of the plasma to obtain inverted populations. The problem of designing an experiment to demonstrate gain is twofold. The first is to measure and match the actual plasma conditions to the choice of laser pulse time history, target composition and geometry. The second is to produce a convincing diagnostic for enhanced stimulated emission in the absence of regenerative feedback. In most current experiments the measurement of plasma conditions is emphasized. It appears that more work can usefully be applied to the problem of gain diagnosis.

The development of soft x-ray laser action will undoubtedly stimulate considerable development in x-ray materials and recording technology. Whether effecitve methods for regenerative feedback are developed from this may not limit the applications for lasers in this wavelength range, however. In particular, the generation of coherent energy by nonlinear optical techniques is presently being extended into the extreme vacuum ultraviolet.[33] The use of such techniques with a soft x-ray amplifier[31] could hasten many exciting applications[34] for a source of high power, coherent x-rays.

REFERENCES

1. A. Javan, W.R. Bennett, Jr. and D.R. Herriott, Phys. Rev. Lett. 6, 106 (1961).
2. M.J. Bernstein and G.G. Comisar, J. Appl. Phys. 41, 729 (1970).
3. I.N. Knyazev and V.S. Letokhov, Opt. Comm. 3, 332 (1971).
4. L. Spitzer, Physics of Fully Ionized Gases, Interscience (New York, 1967).
5. H.R. Griem, Plasma Spectroscopy, (McGraw-Hill, New York, 1964).
6. L.I. Gudzenko and L.A. Shelepin, JETP 18, 998 (1964), also, L.I. Gudzenko and L.A. Shelepin, soviet Phys. Doklady 10, 147 (1965).
7. W.L. Bohn, Appl. Phys. Lett. 24, 15 (1974).
8. K.G. Whitney and J. Davis, J. Appl. Phys. 45, 5294 (1974).
9. T.C. Bristow, M.J. Lubin, J.M. Forsyth, E.B. Goldman, and J. Soures, Opt. Comm. 5, 315 (1972).
10. R.C. Elton, Appl. Optics 14, 97 (1975).
11. W.W. Jones and A.W. Ali, NRL Memorandum Report 2999, U.S. Naval Research Laboratory, 1975; also A.W. Ali and W.W. Jones, NRL Memorandum Report 3015, U.S. Naval Research Laboratory, 1975.
12. R.A. Andrews, R.C. Elton, J. Reinjes, R.C. Eckardt, R.H. Lehmberg, R. Waynant, T.N. Lee, L.J. Palumbo, J.M. McMahon, D. Nagel, and W. Jones, NRL Memorandum Report 2910, U.S. Naval Research Laboratory, 1974.
13. F.E. Irons and N.J. Peacock, J. Phys. B 7, 441 (1974).
14. P. Jaegle, A. Carillon, P. Dhez, G. Hamelot, A. Sureau and M. Cukier, Phys. Lett. 36A, 167 (1971).

15. P.J. Mallozzi, H.M. Epstein, R.G. Jung, D.C. Appelbaum, B.P. Fairand, W.J. Gallagher, and B.E. Campbell, Paper presented at VIII International Conference on Quantum Electronics (Post-deadline Paper), San Francisco, 1974.

16. A. Carillon, G. Jamelot, A. Sureau, and P. Jaegle, Phys. Lett. 38A, 91 (1971).

17. B.A. Norton and N.J. Peacock, J. Phys. B 8, 989 (1975).

18. M. Oron and Y. Paiss, Rev. Sci. Inst. 44, 1293 (1973).

19. J. Soures, L.M. Goldman and M. Lubin, Nuclear Fusion 13, 6 (1973).

20. P.J. Mallozzi, H.M. Epstein, R.G. Jung, D.C. Applebaum, B.P. Fairand, and W.J. Gallagher, in Fundamentals of Applied Laser Physics, edited by M.S. Feld, A. Javan, and N.A. Kurnir, (Wiley Interscience, New York, 1973) pp. 165-220.

21. D.J. Nagel, P.G. Burkhalter, C.M. Dozier, J.F. Holzrichter, B.M. Klein, J.M. McMahon, J.A. Stamper and R.R. Whitlock, Phys. Rev. Lett. 33, 743 (1974).

22. R.C. Elton, NRL Memorandum Report 6738, U.S. Naval Research Laboratory, 1968.

23. A.G. Hearn, Proc. Phys. Soc. 81, 648 (1963).

24. H.R. Griem, Spectral Line Broadening by Plasmas, Academic Press, New York (1974).

25. M. Galanti, N.J. Peacock, B.A. Norton and J. Puric, Proc. Fifth IAEA Plasma-Fusion Cone, Tokyo (1974).

26. C.R. Vidal, J. Quant. Spectrosc. Radiation Transfer 6, 461 (1966).

27. D. Inglis and E. Teller, Astrophys. J. 90, 439 (1939).

28. H.J. Kunze, A.H. Gabriel and H.R. Griem, Phys. Fluids 11, 662 (1968).

29. E. Bliss, G. Sommargren, H.J. Weaver, D.R. Speck, J. Holzrichter, J. Erkkila and A. Gross, Laser Program Annual Report, Lawrence Livermore Laboratory, 1974, pp.191-197.

30. A.H. Gabriel, Mon. not. R. Astr. Soc. 160, 99 (1972).

31. R.A. Andrews, R.C. Elton, J. Reintjes, T. Lee and R. Eckardt, NRL Memorandum Report 3057, U.S. Naval Research Laboratory, 1975.

32. Yu A. Bykovskii, Yu P. Kozyrev, S.M. Silnov, and B. Yu Sharkov, Sov. J. Quantum Electron. 4, 405 (1974).

33. D. M. Bloom, G.W. Bekkers, J.F. Young and S.E. Harris, Applied Phys. Lett. 26, 687 (1975); see also A.H. Kung, J.F. Young and S.E. Harris, Appl. Phys. Lett. 22, 301 (1973).

34. G.C. Bjorklund, S.E. Harris and J.F. Young, Appl. Phys. Lett. 25, 451 (1974).

FIGURE CAPTIONS

Fig. 1 The early evolution of a plasma produced by irradiation of a solid surface by a very high power laser pulse. In (a) the solid surface is shown prior to irradiation. As the laser pulse is incident a narrow region of ionized particles forms near the surface as in (b). Absorption of energy continues and a hot plasma is formed with approximately the density profile shown in (c).

Fig. 2 Representative electron temperature and density profiles in a neodymium laser plasma. The abscissa measures the distance from the solid surface in microns. The four regions indicated are discussed in the text.

Fig. 3 Energy level diagram for proposed population inversion in helium-like oxygen.

Fig. 4 Energy level diagram for proposed population inversion in carbon-like ions.

Fig. 5 Relative transmission coefficient of thin aluminum foils for bremsstrahlung x-rays produced at various temperatures.

Fig. 6 Predicted line intensity ratio of the hydrogen-like resonance line (L_α) to the helium-like resonance line (w) in an aluminum plasma. The predictions of both the corona and collisional radiative (CR) models are shown.

Fig. 7 Predicted line intensity ratio of the helium-like resonance line (w) to intercombination line (y) as a function of electron density in an aluminum plasma at two temperatures.

Fig. 8 Schematic diagram of a multi-stage Nd^{+3}:glass laser system used in laser plasma x-ray experiments at the University of Rochester.

Fig. 9 Simple crystal spectrometer used in laser plasma experiments.

Fig. 10 Microdensitometer trace of the spectrum of an aluminum plasma produced by a focussed, 7.9 joule, 10^{-10}sec. pulse from the laser shown in Fig. 7. The spectrum was recorded on the instrument shown in Fig. 8.

TABLE 1

SYSTEM	ION	TRANSITION	WAVELENGTH	LIFETIME,SEC.
He-Ne Laser	Ne	5s→3p	6328Å	10^{-8}
Ar-Ior Laser	Ar^{+}	4p→4s	4880Å	10^{-8}
Laser Plasma	O^{+6}	3p→2s	128Å	10^{-11}
Laser Plasma	Al^{+12}	2p→1s	7.17Å	10^{-12}

Approximate excited state lifetimes for visible laser transition and representative soft x-ray transitions in laser produced plasmas.

TABLE 2

System	Plasma	T_e,ev	n_e,cm^{-3}	τ_{ee},sec.	τ_{ei},sec.
He-Ne Laser	He^{+}	0.5	$3x10^{11}$	10^{-4}	10^{-2}
CO_2 Laser (atm.)	He^{+}	4.0	10^{13}	10^{-6}	10^{-4}
Ar-Ion Laser	Ar^{+}	3.0	10^{14}	10^{-7}	10^{-5}
CO_2 Laser Plasma	Al^{+13}	10^{3}	10^{19}	10^{-10}	10^{-8}
Nd Laser Plasma	Al^{+13}	10^{3}	10^{21}	10^{-12}	10^{-10}

Approximate electron and electron-ion thermalization times predicted by equations 1 and 2 for representative electric discharge lasers and laser-produced plasmas.

TABLE 3

System	Ion	Transition	Wavelength	$\Delta\nu$,Hz	$\Delta\nu/\nu$
He-Ne Laser	Ne	5s→3p	6328Å	10^9	10^{-6}
Ar-Ion Laser	Ar^+	4p→4s	4880Å	10^{10}	10^{-5}
CO_2 Laser (atm)	CO_2	$00^0 1 \rightarrow 10^0 0$	10.6μ	10^9	3×10^{-4}
Laser Plasma	O^{+6}	3p→2s	128Å	10^{14}	3×10^{-4}
Laser Plasma	Al^{+12}	2p→1s	7.17Å	10^{15}	2×10^{-4}

Approximate transition linewidths for representative electric discharge lasers and typical laser-produced plasmas.

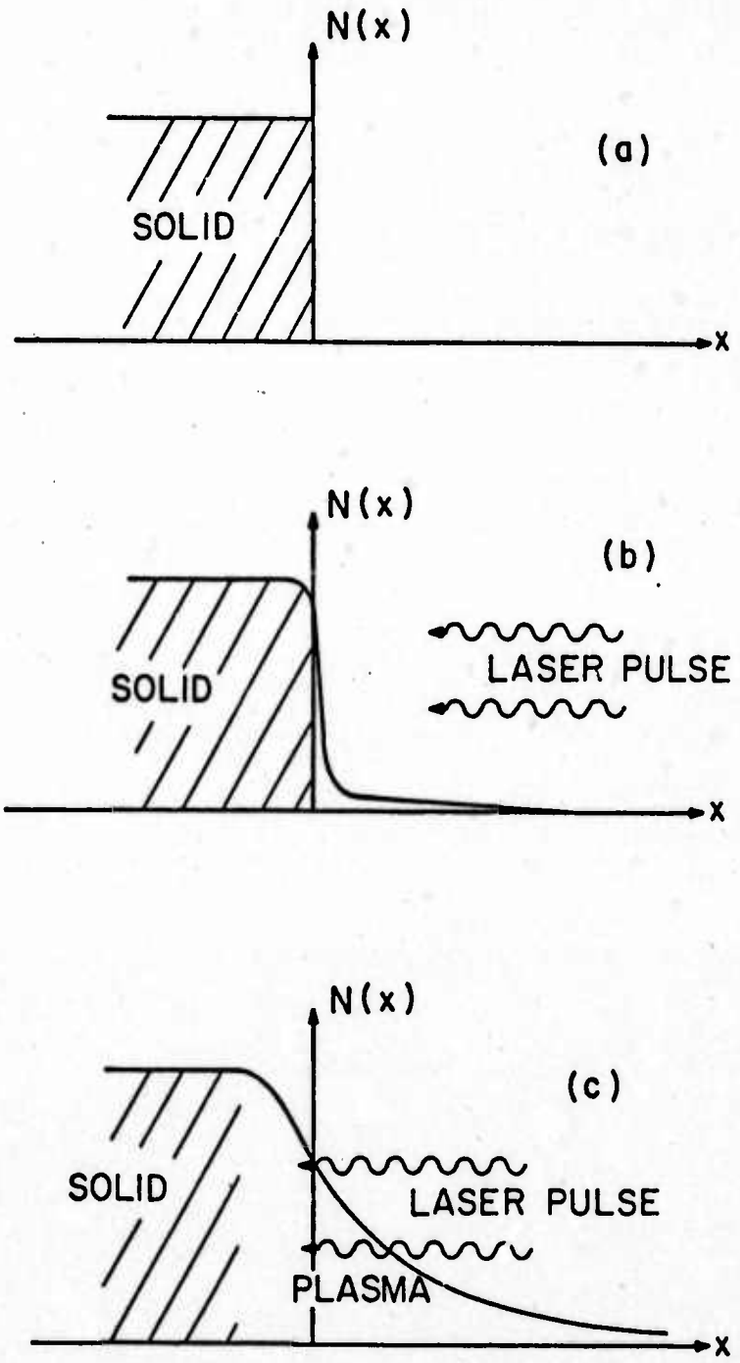
N(x)
(a)
SOLID
x
N(x)
(b)
SOLID
LASER PULSE
x
N(x)
(c)
SOLID
LASER PULSE
PLASMA
x

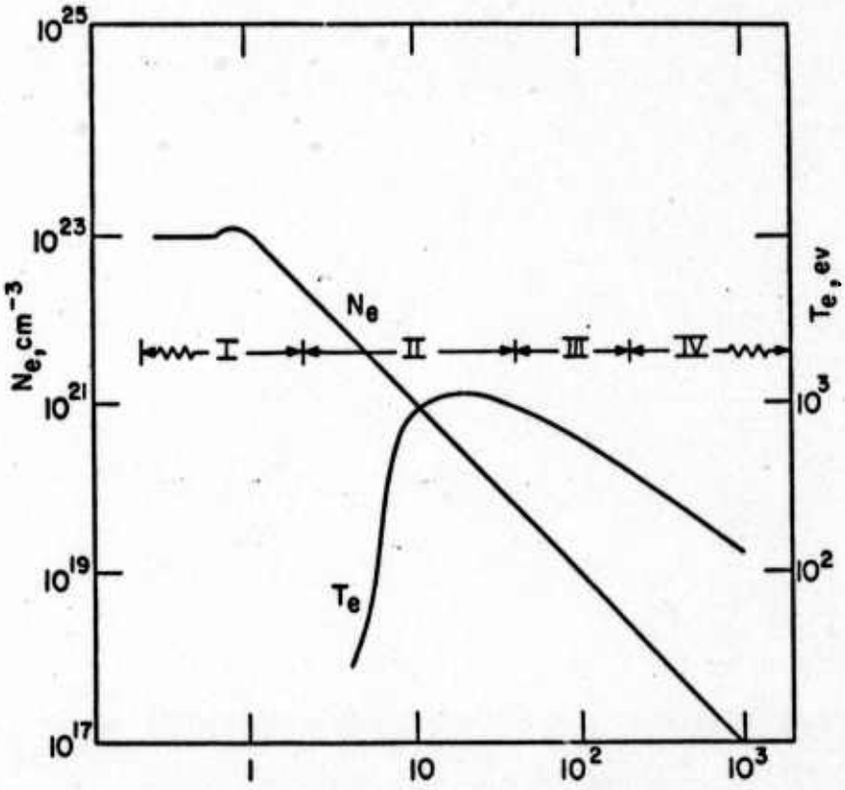
10^{25}
10^{23}
10^{21}
10^{19}
10^{17}
N_e, cm^{-3}
N_e
I
II
III
IV
T_e
10^3
10^2
T_e, ev
1
10
10^2
10^3
DISPLACEMENT FROM ORIGINAL
TARGET SURFACE, MICRONS

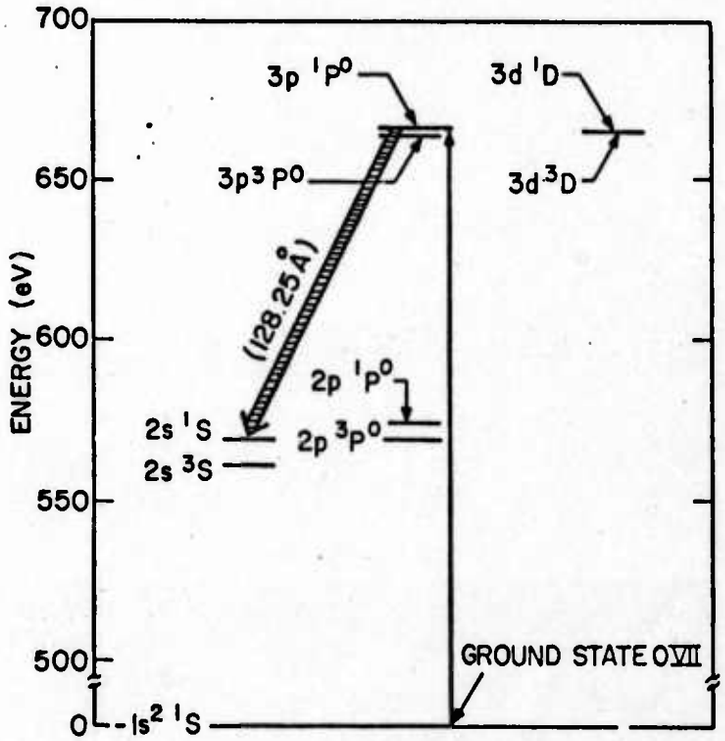
700
650
600
550
500
0
ENERGY (eV)
3p ¹P⁰
3d ¹D
3p³P⁰
3d³D
(128.25 Å)
2p ¹P⁰
2s ¹S
2p³P⁰
2s³S
GROUND STATE OVII
1s² ¹S

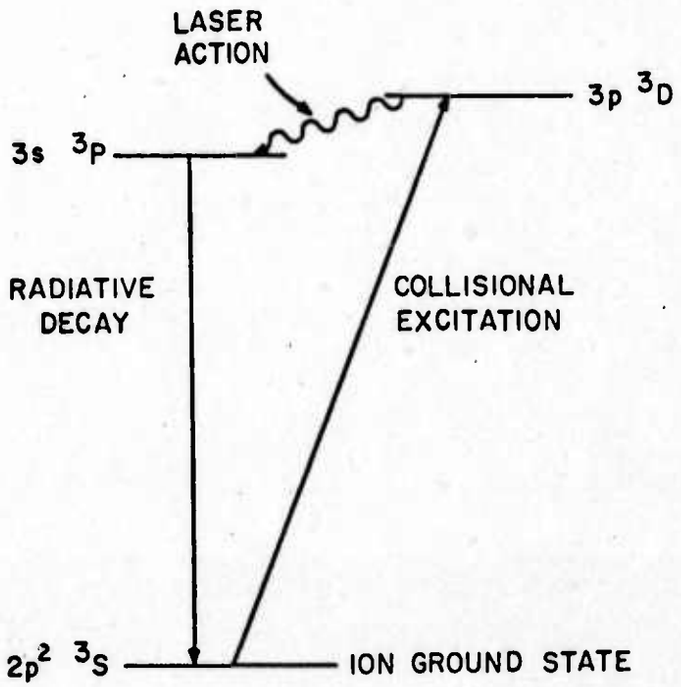
LASER
ACTION
3p ^{3}D
3s ^{3}P
RADIATIVE
DECAY
COLLISIONAL
EXCITATION
2p^2 ^{3}S
ION GROUND STATE

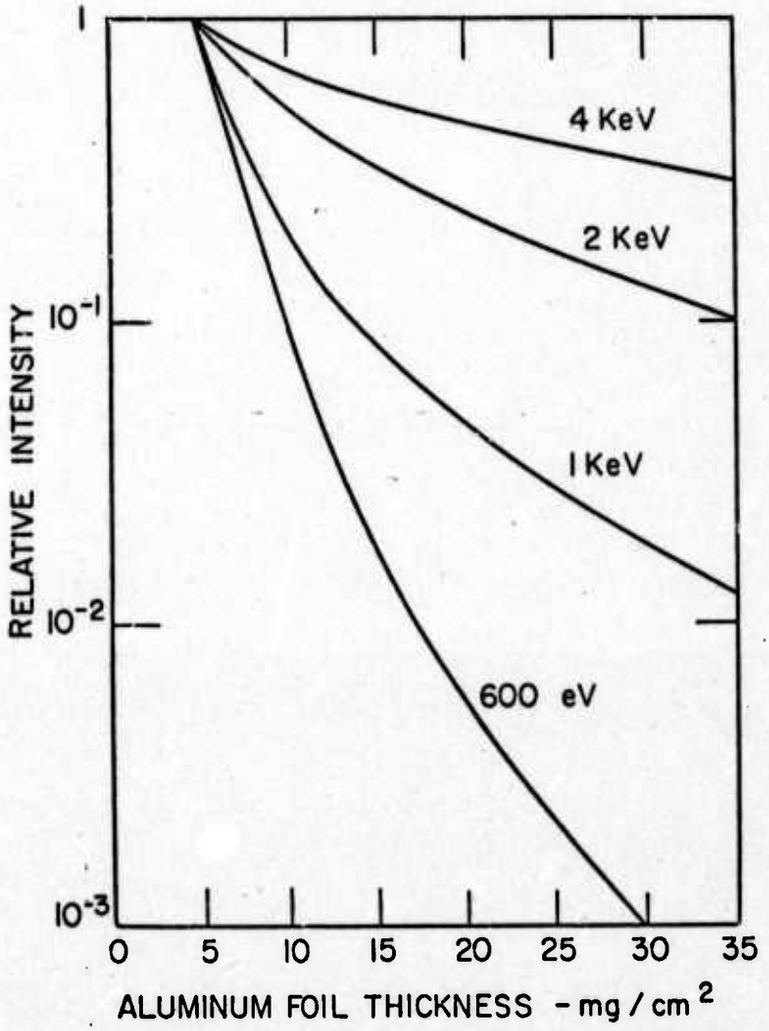
1
10^{-1}
10^{-2}
10^{-3}
RELATIVE INTENSITY
4 KeV
2 KeV
1 KeV
600 eV
0
5
10
15
20
25
30
35
ALUMINUM FOIL THICKNESS - mg / cm 2

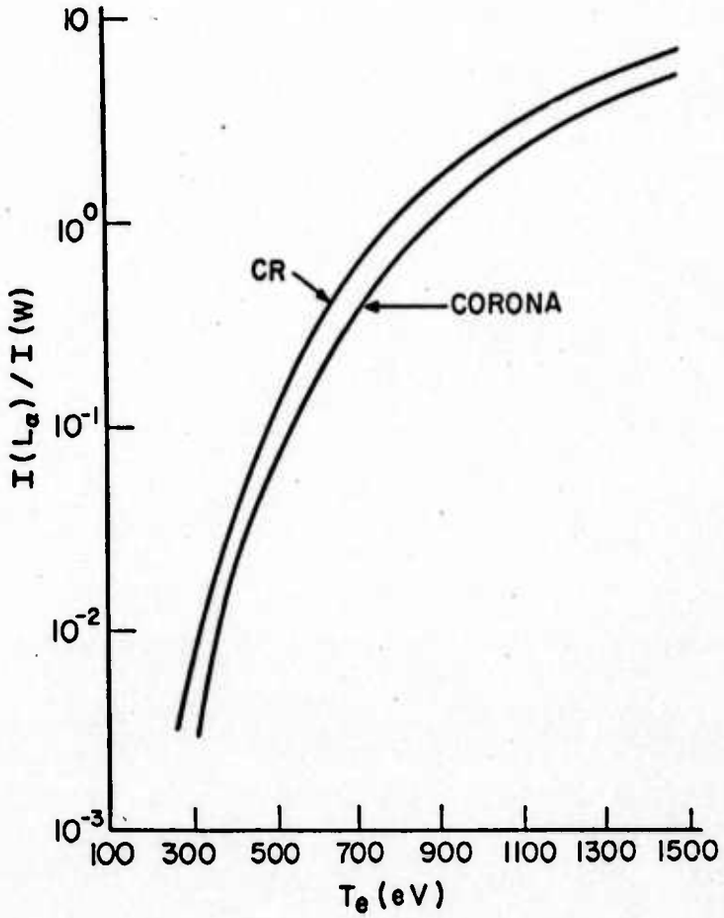
10
10^0
10^{-1}
10^{-2}
10^{-3}
$I(L_\alpha)/I(W)$
CR
CORONA
100 300 500 700 900 1100 1300 1500
T_e (eV)

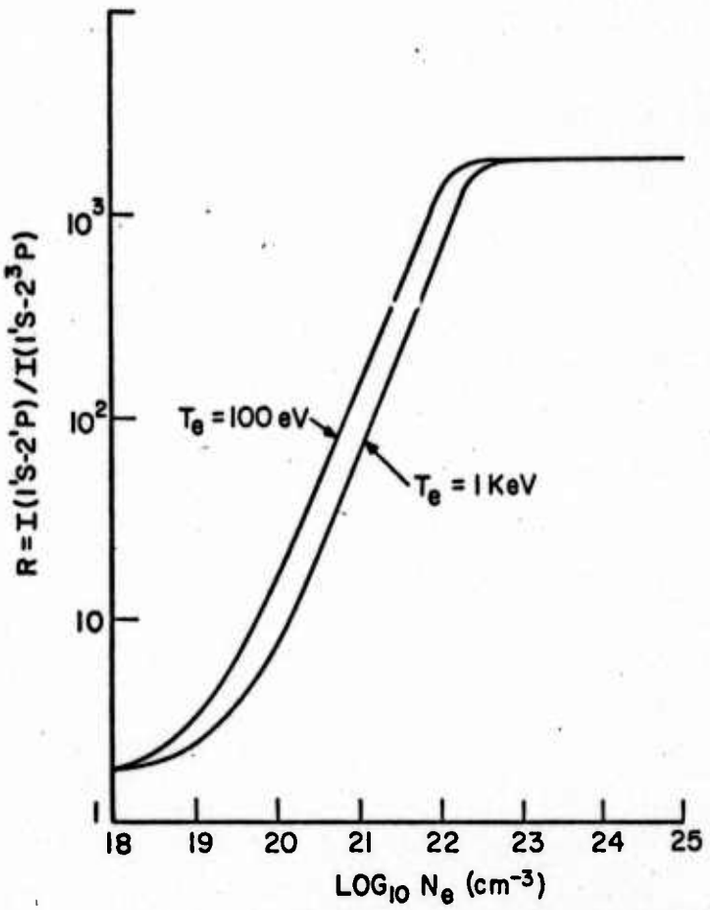
R = I(1'S-2'P)/I(1'S-2³P)
10³
10²
10
1
T_e = 100 eV
T_e = 1 KeV
18
19
20
21
22
23
24
25
LOG₁₀ N_e (cm⁻³)

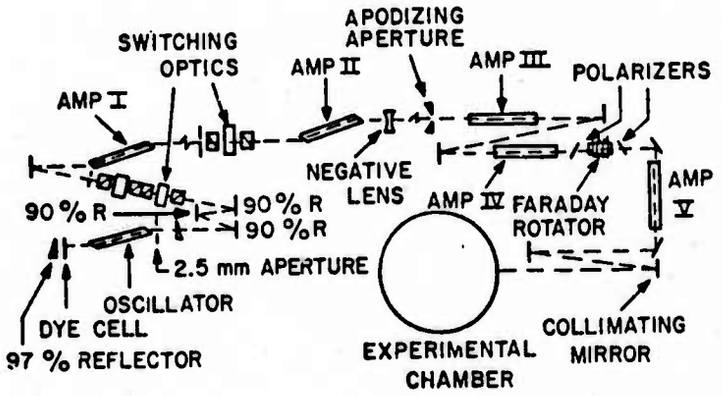
SWITCHING
OPTICS
APODIZING
APERTURE
AMP II
AMP III
POLARIZERS
AMP I
NEGATIVE
LENS
AMP IV
FARADAY
ROTATOR
AMP
V
90 % R
90 % R
90 % R
2.5 mm APERTURE
OSCILLATOR
DYE CELL
97 % REFLECTOR
EXPERIMENTAL
CHAMBER
COLLIMATING
MIRROR

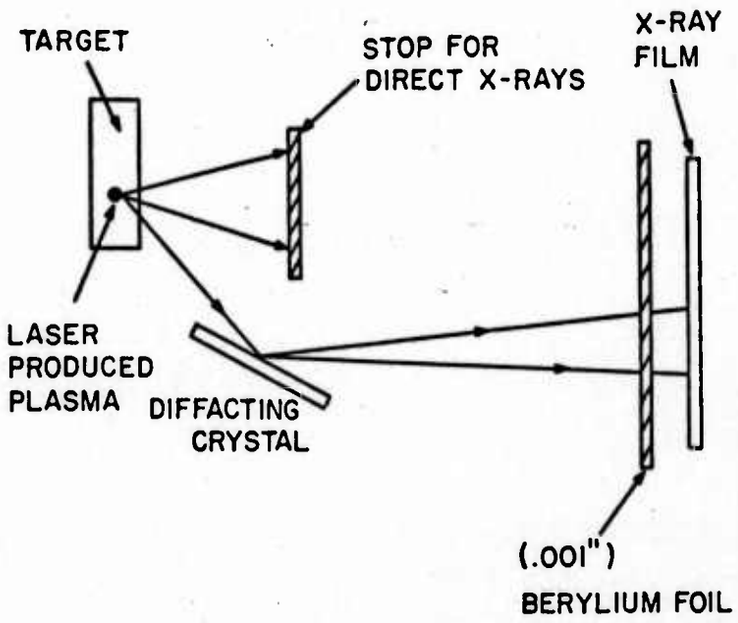
TARGET
STOP FOR
DIRECT X-RAYS
X-RAY
FILM
LASER
PRODUCED
PLASMA
DIFFACTING
CRYSTAL
(.001")
BERYLIUM FOIL

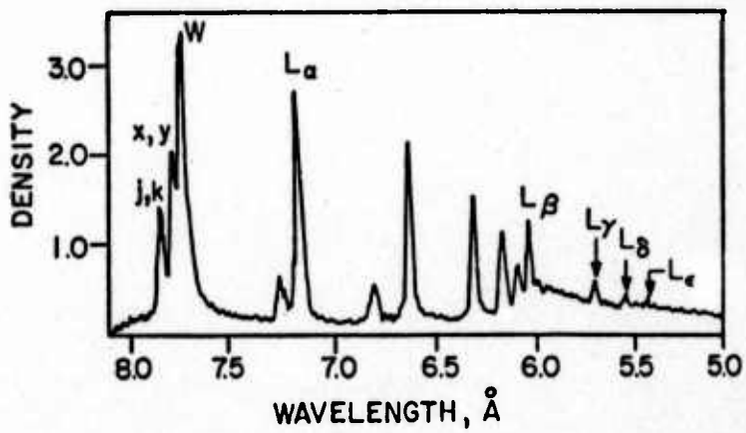
W
L_α
x, y
j, k
L_β
L_γ
L_δ
L_ϵ
3.0
2.0
1.0
DENSITY
8.0
7.5
7.0
6.5
6.0
5.5
5.0
WAVELENGTH, Å